CoFe Prussian Blue Coordination Compounds Incorporating Metallopolymers: Investigation of Electrocatalytic Water Oxidation Activities

A thesis submitted to
the graduate school of engineering and science
of Bilkent university
in partial fulfillment of the requirements for
the degree of
Master of Science
in
Chemistry

By

Merve Demirkıran

February 2016

CoFe Prussian Blue Coordination Compounds Incorporating Metallopolymers: Investigation of Electrocatalytic Water oxidation Activities

By Merve Demirkıran

We certify that we have read this thesis and that in our opinion it is fully adequate, in scope and in quality, as a thesis for the degree of Master of Science.

Ferdi Karadaş (Advisor)

Ömer Dağ

Yavuz Dede

Approved for the Graduate School of Engineering and Science:

Levent Onural
Director of the Graduate School

ABSTRACT

CoFe Prussian Blue Coordination Compounds Incorporating Metallopolymers: Investigation of Water Oxidation Activities

Merve Demirkıran

M.S. in Chemistry

Advisor: Ferdi Karadaş

February 2016

Hydrogen economy, which depends on water and sunlight as energy source, needs to be implemented as an alternative to carbon based economy. For the development of a technology that incorporates hydrogen energy to our daily lives, it is required to split the water with the help of an efficient water oxidation catalyst. CoFe Prussian Blue analogues have recently been investigated as heterogeneous water oxidation catalysts. Even though they exhibit they exhibit high electrocatalytic activity in addition to superior stability in both acidic and neutral media low current densities were obtained with CoFe PB modified FTO electrodes due to their low surface coverage. This challenge could be overcome by developing novel synthetic methods that will enforce the formation of amorphous CoFe Prussian Blue analogues.

Herein this thesis, pentacyanoferrate based metallopolymers were used as precursors to prepare amorphous Co-Fe analogues. The project focuses on the improving surface concentration by using Poly 4-vinyl pyridine (P4VP) not only as a capping ligand connected

to pentacyanoferrate complexes but also as a surfactant to prevent the formation of long-range ordering between Co-Fe networks. Surface concentration was improved approximately seven fold, which resulted in an increase in the catalytic activity. A current density of 1 $mA.cm^{-2}$ was obtained only at η = 510 mV while the same current density could be obtained only at higher overpotentials (>600 mV) with the previously studied Prussian Blue analogues. The stability of CoFe-PVP coated FTO electrodes were investigated before and after the electrocatalytic process using Infrared, XPS, and EDX studies. The results of this study indicate that the rich and diverse chemistry of pentacyanoferrates make them potential candidates for application in heterogeneous water oxidation catalysis.

Keywords: Water Oxidation Catalyst, Prussian Blue, amorphous structure, current density

ÖZET

Metalpolimerlere birleştirilen CoFe Prusya Mavisi Koordinasyon Bileşikleri: Elektrokatalitik su oksidasyon aktivitelerinin incelenmesi

Merve Demirkıran
Kimya, Yüksek Lisans
Tez Danışmanı: Ferdi Karadaş
Şubat 2016

Enerji kaynağı olarak sadece su ve güneş ışığına bağlı olan hidrojen ekonomisinin, karbon bağımlı ekonomiye alternatif olarak geliştirilmesine ihtiyaç duyulmaktadır. Hidrojen enerjisini günlük hayatımıza sunacak teknolojinin gelişmesi için, suyu parçalamakta rol alacak verimli bir su oksitleyen katalizöre gerek vardır. Hem asidik, hemde nötr ortamlarda dayanıklılık ve sağlamlıkları nedeniyle, Co-Fe prusya mavisi analogları heterojen su oksitleyen katalizörler olarak son zamanlarda incelenmektedir. Hekzasiyanoferrat merkezli Co-Fe PB koordinasyon polimerinin, düşük yüzey konsantrasyonlarından dolayı düşük akım yoğunluğuna sahip olmaları, başlıca dezavantajıdır ve bu problem aşmak için yeni bir sentez yöntemi geliştirmek gerekmektedir. İyi bilinen pentasiyanoferrat kimyasının yardımıyla, amorf Co-Fe PB analoglarının hazırlanması ve pentasiyanoferrat bazlı metalpolimerlerin

sentezlenmesi, düşük yüzey konsantrasyonu sorununun üstesinden gelinmesi için mümkündür. Bu tezde sunulan çalışma, P4VP polimerinin, pentasiyanoferrat komplekslerine substrat olarak bağlanıp, Co-Fe kristal parçacıklarının büyümesini bir dereceye kadar engellemesi için surfaktan olarak kullanılmasıyla yüzey konsantrasyonunun geliştirilmesi üzerine odaklanmaktadır. Yüzey konsantrasyonu yaklaşık 7 kat artırılmış ve bu artış katalitik aktivitede de artışa neden olmuştur. 1 mA./cm-2 akım yoğunluğu, daha önce çalışılmış PB analoglarıyla daha yüksek aşırı potansiyellerde (>600 mV) elde edilirken, aynı akım yoğunluğu değeri sadece η = 510 mV aşırı potansiyelde elde edilmiştir. Elektrotların kararlılıklarını incelemek için, elektrokatalitik aktivasyonlarının öncesinde ve sonrasında IR ve EDX analizleri yapılmıştır. Çalışmaların sonuçları, zengin ve çeşitli pentasiyanoferrat kimyasının, Co-Fe PB analoglarını heterojen su oksidasyon katalizör uygulamalarında potansiyel aday yaptığını göstermektedir.

Anahtar sözcükler: Su oksitleyici katalizör, Prusya Mavisi, amorf yapı, akım yoğunluğu.

Acknowledgement

Firstly, I would like to express my special thanks to my advisor Assist. Prof. Ferdi Karadaş, for his support for my master studies with his guidance, motivation, always smiling face and profound knowledge. Although I usually made too much trouble for him because of my lasting questions and dissatisfactions, he always had a satisfactory answer with his lasting patience. I cannot stop myself from screaming "hocaaaaam" loudly in excitement, every time I see him and other members in lab start to imitate me to make fun of my loud excitement.

Besides my advisor, I would like to thank the rest of my thesis committee. Prof. Dr. Ömer Dağ, and Assoc. Prof. Yavuz Dede for their insightful comments and encouragement.

My sincere thanks also goes to Dr. Satya Vijay Kumar Nune (The DUDE), who always fond the way of cheer me up and encourage me. You were always with me in the worst time of my life. How lucky am I, to be trained by a person like you to deal with my troubles. My special thanks to my colleagues in the lab, Dr. Rupali Mishra, Pınar Alsaç, Aysun Tekin and Büşra Altınsoy for their role that make the experiences more enjoyable.

I am so grateful to my family for their support from my early youth up to now. Thanks are in due to the Aksoy family, for their intimate love and support. My special thanks to my friends Aylin, Esra, Lütfiye, Obadah, Büşra and Merve, for their encouragement and support over the years.

Finally my heartfelt gratitude to my dear husband. Your encouragement when the times got rough is much appreciated. It was a great comfort to know that you support my decisions and inspire me to do more.

To My Family

“Attraversiamo”

Contents

List of Figures

List of Tables

Abbreviations

Γ	Surface coverage
η	Overpotential
λ	Wavelength
μ	Micro
ν	Wavenumber
υ	Potential scan rate
A	Ampere
A	Area
Bpy	2,2-bipyridine
C	Coulomb
CoHCF	Cobalt hexacyanoferrate
$CoFe(CN)_6$	Cobalt Hexacyanoferrate catalyst
$CoFe(CN)_5$-P4VP	Cobalt Pentacyanoferrate coordinated P4VP
$CoFe(CN)_5$-P4VP@FTO	Cobalt Pentacyanoferrate coordinated P4VP on FTO
$CoFe(CN)_6$@FTO	Cobalt Hexacyanoferrate on FTO
CoPi	Cobalt Phosphate
CV	Cyclic voltammetry
EDX	Electron Dispersive X-ray spectroscopy
E	Potential
E_o	Standard redox potential

$E_{1/2}$	Half-wave potential
F	Faraday's constant
$Fe(CN)_5$-NH_3	Sodium aminopentacyanoferrate
$Fe(CN)_6$	Potassium hexacyanoferrate as catalyst
$Fe(CN)_5$-P4VP	P4VP coordinated pentacyanoferrate
I	Current
IR	Infrared spectroscopy
ITO	Tin doped indium oxide
FTO	Fluorine doped Tin Oxide
j	Current density
K	Kelvin
k_{cat}	Effective first-order rate constant
KPi	Potassium phosphate
M	Molar
$M(CN)_6$	Metal hexacyanoferrate
MHCM	Transition metal hexacyanometallates
MLCT	Metal to ligand charge transfer
NHE	Normal Hydrogen Electrode
OEC	Oxygen evolving complex
PB	Prussian blue
PCET	Proton Coupled ElectronTransfer
P4VP	Poly 4-vinylpyridine
Py	Pyridine
Pz	Pyrazine
RT	Room Temperature

SEM	Scanning electron microscopy
TOF	Turnover frequency
UV-Vis	Ultraviolet-visible spectroscopy
V	Volt
WOC	Water Oxidation Catalyst
XRD	X-ray Diffraction
XPS	X-ray Photoelectron Spectroscopy

Chapter 1

INTRODUCTION

1.1. Today in Energy

Global energy demand has been going up steeply each year and expected to double by 2050 because of the growing population, needs, and technological development [1]. Although the energy requirement could be met from the commonly used fossil based fuel deposits in the near future, increased CO_2 level in the atmosphere poses bigger challenges to the environment such as global warming and climate change, thus, resulting in raising sea level and pH decrease in the ocean [2]. The aforementioned scenario could be avoided by developing clean and renewable alternatives to fossil fuels, which are carbon free, viable, and environment friendly [3].

Hydrogen is one of the candidates as a clean burning fuel since it has the highest energy per mass density of any fuel (144 MJ/kg) and produces only water as a product [4]. Thus, smart technologies should be developed to produce hydrogen from electrolysis of water with the help of efficient and robust water oxidation catalysts (WOCs) [5] .Water splitting occurs in nature to supply protons and electrons to the photosystem and to release oxygen to the atmosphere. By following the lead of the nature [6], it is the water oxidation step which imposes significant overpotentials to the system since it requires $4e^-$ and $4H^+$ transfers to form an oxygen-oxygen bond. The half reactions with reduction potentials are shown below:

$2H_2O \leftrightarrow O_2 + 4e^- + 4H^+$; $E_{anodic} = 1.23 - 0.059\times(pH)$ V (vs. NHE)

$4e^- + 4H^+ \leftrightarrow 2H_2$; $E_{cathodic} = 0 - 0.059\times(pH)$ V (vs. NHE)

Since water oxidation requires high potentials, the current research in this field has mainly been focusing on the development of novel WOCs.

1.2. Water Oxidation Catalysts (WOCs)

The development of stable, inexpensive, and fast WOCs has been one of the main issues especially in the last three decades [7, 8]. Since it is easier to carry out mechanistic studies on molecular water oxidation catalysts, they have been prepared as model catalysts to elucidate the electronic properties required for high catalytic activity [9, 10] .Heterogeneous solid state water oxidation catalysts have also been designed and developed to use the advantage of their stability, robustness, and easier adaptation to the devices [11].

Among the WOCs studied up to date, cobalt based WOCs have made the richest contribution to the field due to their diversity and high catalytic efficiency especially in neutral and basic media [12, 13]. The reported oxide and nonoxide cobalt based WOCs will be discussed along with their advantages and disadvantages in the upcoming section.

1.3. Cobalt based WOCs

1.3.1. Oxide WOCs

The most important contribution to the field was made by D. G. Nocera. He discovered highly-active cobalt phosphate (CoPi) thin film, which is formed electrochemically on an ITO substrate from phosphate-buffered solution having Co^{2+} ions [14-16] . The CoPi catalyst is described as layered $(CoO_x)_n$ clusters in molecular dimension which are stabilized by the presence of phosphate groups. Here, the equilibrium between the Co^{2+} and HPO_4^{2-} ions in the solution and Co^{3+}

and HPO_4^{2-} on the cathode electrode prevents the system from Co leaching and helps the catalyst via a self-repair mechanism. It is able to generate O_2 with a moderate overpotential, at neutral pH, 1 atm of pressure, and room temperature when electrolysis was carried out. At 1.29 V (vs. NHE), the current density is more than 1 mA/cm^2 even after approximately 8 hours ([Co^{2+}] = 0.5 mM, 0.1 mM KPi electrolyte, pH = 7) (Figure 1.1). The study was later followed by implementing CoPi systems to silicon-based light-harvesting semiconductors resulting in enhanced OER activity [17, 18].

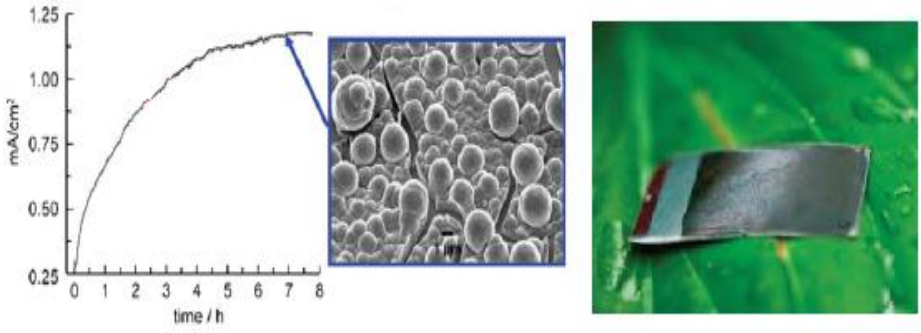

Figure 1.1. Current density graph with the SEM image (Left) and Picture (Right) of the electrodeposited CoPi catalyst film [15, 19].

The mechanism of the oxygen evolution reaction (OER) by CoPi catalyst was studied by electrokinetic experiments, which suggest a proton coupled electron transfer (PCET) equilibrium step between Co^{III}-OH and Co^{IV}-O (Figure 1.2) followed by a chemical turnover-limiting O-O bond formation step. Although the details of O-O bond formation mechanism is to be determined, it is suggested that metal atom dopants may decrease the thermodynamic potential of PCET pre-equilibrium step, promote O-O bond formation, and thus, may increase the

activity at lower overpotentials [20].

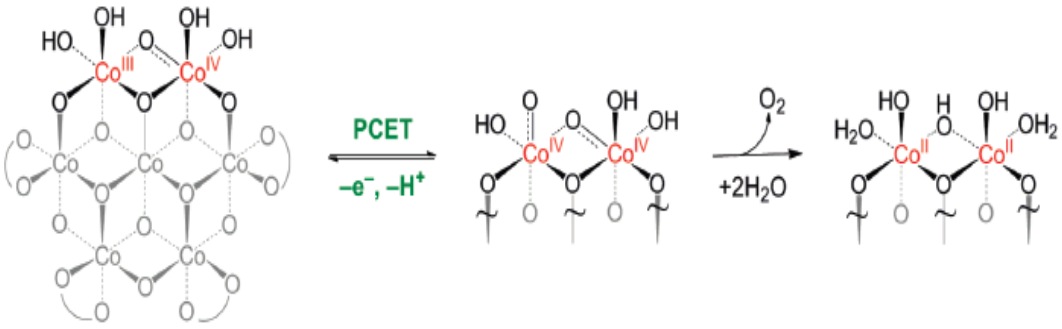

Figure 1.2. Proposed pathway for the OER by CoPi. Curved lines denote phosphate, OH_x terminal or bridging ligands [20].

1.3.2. Non-oxide WOCs

Even though oxide based catalysts have received much attention due to their high catalytic activities, their decomposition at acidic conditions has provoked scientists to investigate also non-oxide catalysts in this field. Berlinguette recently reported such a non-oxide molecular catalyst, Co(**PY5**)(H_2O)](ClO_4)$_2$ (**PY5** = 6-(bis(bis-2-pyridyl)-methoxymethane)pyridine), which contains a single penta-coordinate Co center available for the ligation of water molecule (Figure 1.3., Left). It is considered to be stable against harshly oxidizing conditions since pentadentate ligand framework of **PY5** stabilize the Co metal ion [21].

The PCET step corresponding to the $[Co^{III}\text{-}OH]^{2+}$/ $[Co^{II}\text{-}OH_2]^{2+}$ couple was proved by pH dependence of redox couples oxidation values ($E_{1/2}$) vs NHE between the pH = 2.2-11.7 (Figure 1.3., Right). The significant increase in the current that is consistent with catalytic process was also observed at 1.4 V vs. NHE at pH = 9.2, corresponding to $[Co^{IV}\text{-}OH]^{3+}$ / $[Co^{III}\text{-}OH]^{2+}$ couple. The

experiments performed with fluorescence optical probe at an applied potential 1.59 V vs. NHE over 10 min result in reaction rate coefficient (k_{cat}) of 79 s^{-1}, which is higher than reported values, up to date for molecular catalysts [22].

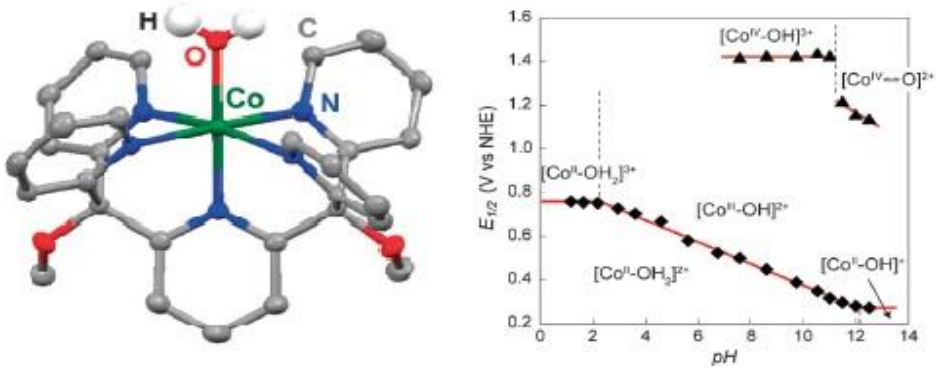

Figure 1.3. Molecular representation of Co(**PY5**)(H_2O)](ClO_4)$_2$ (Left) and Pourbaix diagram of the complex (Right). The counteranion and H atoms are omitted for clarity [21, 22].

Given the success obtained with non-oxide molecular systems, non-oxide heterogeneous catalysts have also been studied. Patzke introduced cobalt carbodiimide (CoNCN) as a new type of heterogeneous non-oxide water oxidation catalyst with dual photochemical and electrocatalytic activities (Figure 1.4.). This material includes Co centers embedded in a nitrogen environment. Because of the interconnected multilayer motif of CoNCN, the delocalization of the holes and the active species diffusion happens rapidly. Its initial TOF value ($TOF/S_{BET} = 2.1\times10^{-1}$ $sec^{-1}.g.m^{-2}$) is higher than that of cobalt oxide ($TOF/S_{BET} = 3.5\times10^{-3}$ $sec^{-1}.g.m^{-2}$). Furthermore, it maintains a constant current density during an electrolysis of more than 20 h [23].

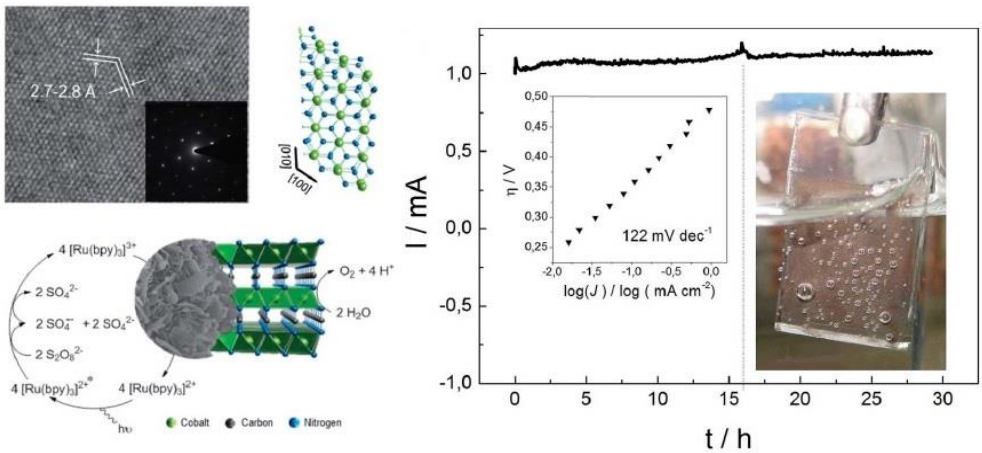

Figure 1.4. HRTEM and SAED pattern of a CoNCN platelet (Left, top). Photocatalytic water oxidation cycle (Left, bottom). Chronoamperometry measurement on a FTO electrode at 1.2 V vs. Ag/AgCl in 0.1 M phosphate buffer (E^0 = 0.62 V vs. Ag/AgCl at pH = 7) (Right). The dotted line indicates mechanical removal of bubbles. The inset shows the Tafel plot with a glassy carbon electrode [23].

1.4. Prussian Blue and Its Analogues

Since it is stable, easily made, intensely colored, and relatively insensitive to the light, it was used by many artists such as Vincent Van Gogh (Figure 1.5), Picasso, and Hokusai [24] as a paint when it was discovered. Although PB and its analogues have been known for more than 300 years, their unusual magnetic [25], electrical [26], optical, and gas storage properties [27] have been investigated mainly in the last 20 years.

Figure 1.5. Vincent van Gogh's "The Starry Night", Saint Rémy, June 1889 [28].

The original Prussian blue is a mixed-valence iron hexacyanoferrate with a formula of $A_{4x}Fe^{III}_4[Fe^{II}(CN)_6]_{3+x}$ $.nH_2O$ (A= alkali metal, $0<x<1$, n=14-16). It has a face-centered cubic crystal structure (Figure 1.6.), in which two different metal centers are bridged by cyanide groups [29].

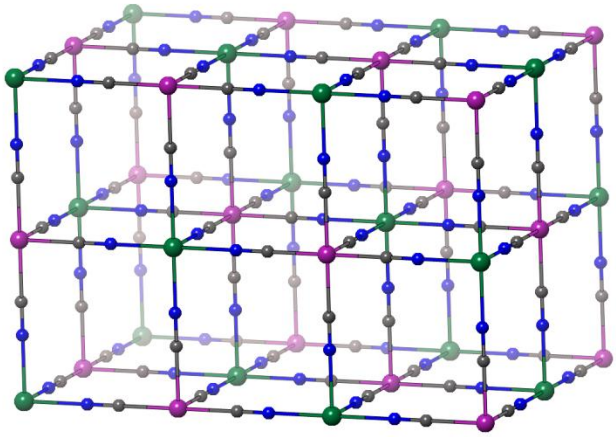

Figure 1.6. Face centered cubic Prussian Blue type crystal structure.

Its isostructural analogues, named as transition metal hexacyanometalates (MHCM), are the compositions of different transition metal ions in multiple oxidation states, which increases the diversity of PB analogues. It is possible to increase the porous nature of PB analogues depending on the charge of reacting groups. When hexacyanometal and metal ion with different charges are reacted, voids in the face-centered cubic structure occur to provide charge balance, which improves the porosity of the network. The voids created by the absence of the $M(CN)_6$ units are filled by the water molecules, which are directly coordinated to metal site.

The deposition and electro-activity of the MHCM as an electrode has also been investigated [30]. They have been used in lithium-ion batteries as efficient anode materials [31]. Furthermore, they have been studied as catalysts for oxidation of organic compounds [32, 33].

1.5. Prussian Blue (PB) analogues as WOCs

Galán Mascarós *et al.* investigated the cobalt hexacyano-ferrate (CoHCF) modified electrodes for their performance in water oxidation catalysis [34, 35]. CoHCF is obtained from the coordination of Co^{2+} ions to $[Fe(CN)_6]^{4-}$ units within a 2:1 mol ratio. Given the literature stating that open Co centers are the reactive sites in water oxidation catalysis, CoHCF is a promising candidate to be used for water oxidation due to its highly porous structure, in which the $M(CN)_6$ cavities are filled by water molecules coordinated to Co centers. In addition, CoHCFs are thermally and chemically stable, easy to synthesize, extremely robust, and they work at neutral pH as well as in acidic conditions.

Galán Mascarós *et al.* prepared CoHCF on FTO-coated glass electrode by applying a well-known electrochemical deposition method. TOF value was found to be 2×10^{-3} s^{-1} at an overpotential of η = 300 mV and 0.5 s^{-1} at 550 mV with a surface concentration of 1.4 ± 0.2 nmol/cm^2. When it was compared with the reported TOF = 2.6 x 10^{-3} s^{-1} value for a cobalt oxide film at η = 410 mV and pH=7, the same value could be obtained at a lower overpotential, η = 305 mV. This difference is referred to different morphology of the film, which changes the surface-to-bulk ratio. On the other hand, the maximum current densities for cobalt oxides are higher because of their higher surface coverage. For cobalt oxides, a current density of 1 mA/cm^2 is obtained with the loading of the active Co sites in the µmol/cm^2 range at η = 400 mV. Galán Mascarós estimates that the same current density value at the same overpotential can be achieved with CoHCF coverages of approximately 2.5 nmol/cm^2. In addition, it was proved that cobalt oxide cannot form at the worked potential range so that the contribution of activity resulting from cobalt oxide formation was invalidated [34].

Similar to Co–Fe PB coordination polymers, Yamada and Fukuzumi *et al.* investigated the photocatalytic activity of heteropolynuclear cyanide complexes, containing cobalt and platinum ions, in water oxidation. They reported the visible light driven water oxidation data of the complexes, in which Co^{III} and Pt^{IV} ions are C-bound and Co^{II} ion is the N-bound to cyanide groups. Here, the N-bound Co^{II} ions are active metal sites and the activity is expected to increase with the addition of $[Pt^{IV}(CN)_6]^{2-}$ units to cobalt cyanide because of the higher oxidation state of Pt^{IV} than Co^{III}. Furthermore the activity again increases when the complex contains coordinatively unsaturated Pt^{II} ions instead of Pt^{IV} since the number of

defect sites result in an increase in the number of active sites [36].

When the number of N-bound metal is higher than C-bound metal, the N-bound metal should bind to other ligands, such as water, to complete the octahedral coordination as explained in both explained studies on PB coordination polymers. This type of metal site, with at least one coordinated water molecule, is called the '*active site*' [37]. The main drawback of the CoHCFs is their relatively lower current densities due to low surface coverage number of active sites, even tough they are robust and stabile in both acidic and neutral media. The reason, for the relatively low number of active sites in cyanide systems, is that most of the cobalt sites in the crystalline framework are connected to six nitrogen atoms of the cyanide group except the ones on the surface and the vacancies, created to provide charge balance. It is, therefore, evident that metal cyanide networks with low or no crystallinities should be prepared to obtain a current density of 1 $mA.cm^{-2}$ at much lower overpotentials.

The following studies on WOCs based on metal cyanide networks should focus on increasing the active Co sites by offering a new synthetic approach with the help of cyanide precursors other hexacyanometals such as well-established pentacyanometal chemistry.

1.6. The Pentacyanometalates

The pentacyanometalate is a well-established chemistry with straightforward synthetic procedures. The commercially available sodium nitroprusside, $Na_2[Fe(CN)_5NO]\cdot 2H_2O$ is used as a starting material to synthesize very hygroscopic sodium aminopentacyanoferrate complex, $Na_3[Fe(CN)_5NH_3]\cdot 3H_2O$ [38].

Since the NH_3 ligand in the $[Fe(CN)_5NH_3]^{3-}$ complex has a labile character, it was used as a precursor to prepare pentacyanoferrate complexes with other N-donor ligands [39].

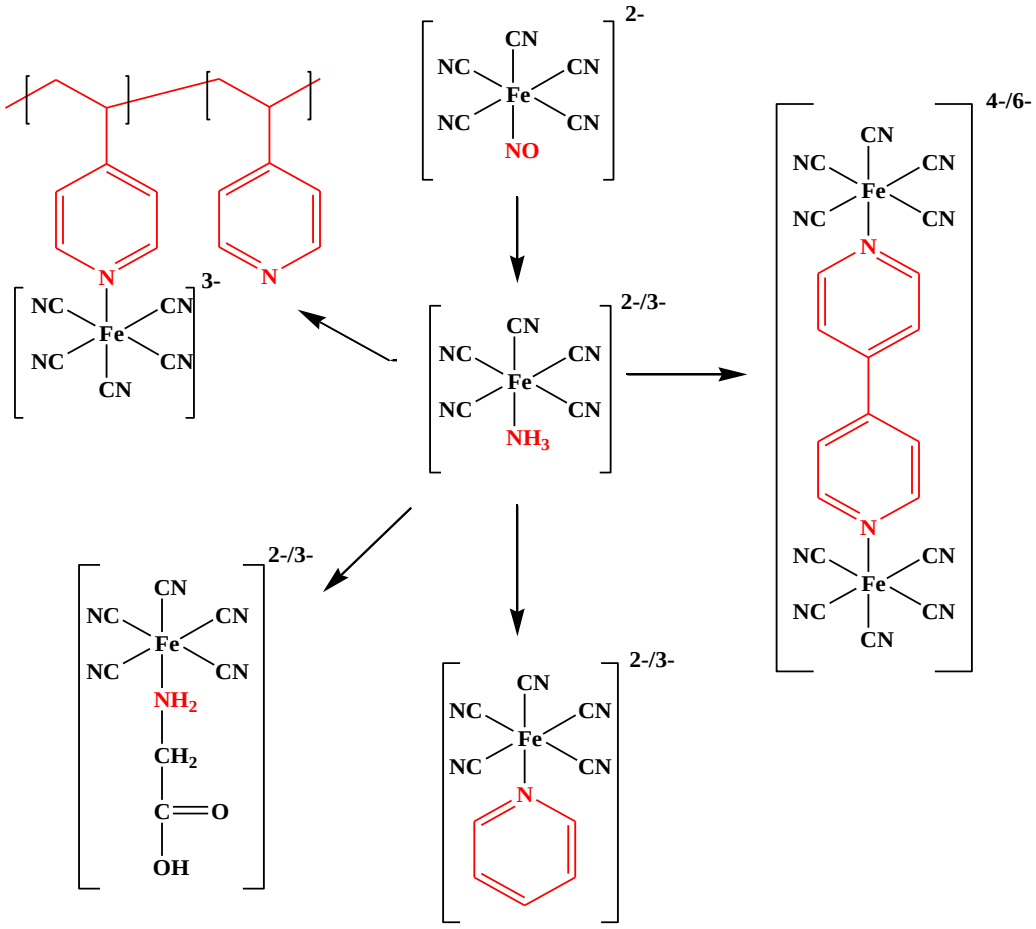

Figure 1.7. Schematic representation of pentacyanoferrates with different N-donor ligands.

The pentacyanoferrate complexes binding to N-donor ligands such as pyridine, bipyridine, pyrazine, amino acid derivatives, and even polymers with available N atoms have been synthesized (Figure 1.7) and their properties has been investigated by using spectroscopic and electrochemical methods since 1970s [40-44].

Moreover, it was proved that PB prepared by using the $[Fe(CN)_6]^{4-}$ as a precursor exhibits a FCC crystal structure, while the precursors $[Fe(CN)_5L]^{3-}$ (L=Py, Pz, Bpy etc.) result in coordination networks with either short-range order or amorphous nature (Figure 1.8). Therefore, the N-donor ligand bound to pentacyanoferrate precursors could be used to reduce the crystallinities of metal cyanide networks and, thus, to increase the number of active metal sites on the surface [45].

Poly 4-vinylpyridine is one of the precursors that could be preferred to bind to pentacyanoferrate complexes to obtain amorphous structure, because it has a long carbon chain which is expected to create steric stabilization to confine the growth of PB particles in the stage of Cobalt addition [46] and dangling pyridine moieties with N-donor atoms that interact with pentacyanoferrate to some extent. The other advantage of pentacyanoferrate coordinated P4VP metallopolymer is to be soluble in water and can be used to produce coated electrodes [47]. And also, the electrochemical response of the pentacyanoferrate coordinated P4VP were published during 1990s [48, 49].

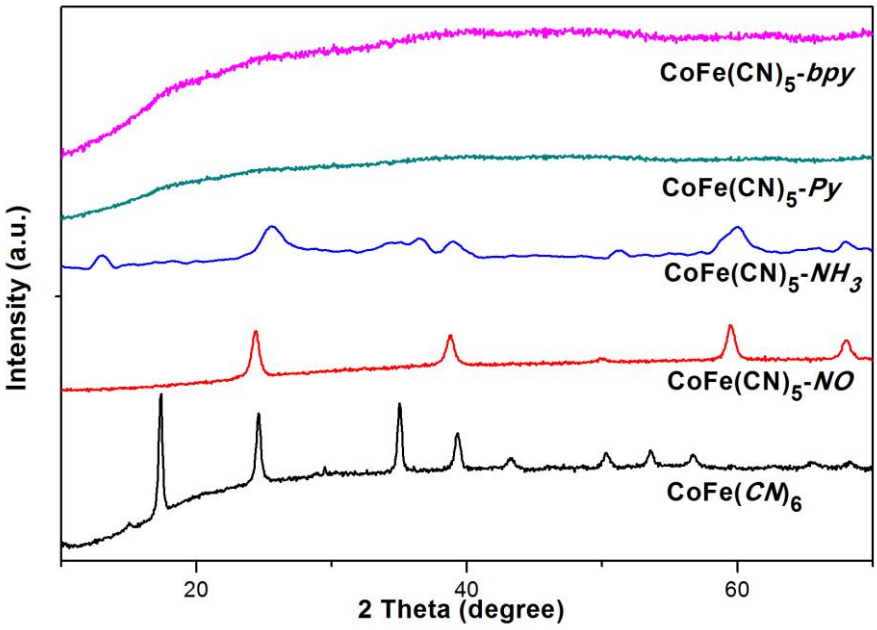

Figure 1.8. XRD patterns of Co-Fe analogues with different N-donor ligands.

1.7. Objective of the Thesis

In this thesis, in the light of well-known pentacyanoferrate chemistry and the previous electrochemical studies on the CoHCF complexes, we offered a novel synthetic approach involving pentacyanometallate based metallopolymers for the preparation of amorphous Co-Fe coordination polymers to increase the number of active metal sites on the surface. It is aimed to obtain metal cyanide coordination compounds with amorphous behavior by using pentacyanoferrate/poly(4-vinylpyridine) hybrid metallopolymers as precursors. Synthesis and characterization of amorphous cobalt pentacyanoferrate/poly(4-vinylpyridine) hybrid compounds is reported. Electrochemical and electrocatalytic water oxidation studies performed on aforementioned samples deposited on FTO electrode is also the focus of this thesis.

Chapter 2

EXPERIMENTAL

2.1. Materials

All the chemicals and solvents used for the synthesis were of analytical grade, obtained from Sigma-Aldrich and used without further purification. The solutions required for the coating purpose of FTO glasses and electrochemical analyses of the samples were prepared with de-ionized water having resistivity of 18 mΩ.

2.1.1. Synthesis of Sodium aminopentacyanoferrate ($Na_3[Fe(CN)_5NH_3].3H_2O$)

$Na_3[Fe(CN)_5NH_3].3H_2O$ was prepared from $Na_2[Fe(CN)_5NO].2H_2O$ (sodium nitroferricyanide) according to the procedure reported in literature [38]. 50 g of $Na_2[Fe(CN)_5NO].2H_2O$ was dissolved in 200 mL of water. 6.7 g of NaOH was added to the solution under constant stirring. NaOH acts as sodium source and also prevent the ammonia from forming ammonium ions to proceed without any secondary product such as a disodium salt, $Na_2NH_4[Fe(CN)_5NH_3]$. The temperature was decreased to 10 ^oC using an ice bath. 25% (v/v) NH_4OH solution (ca. 60 ml.) was added with taking great care not to exceed 20 ^oC. The solution was allowed to stir using magnetic stirrer for 2 hours in an ice bath to make it homogenous, followed by an addition of cold methanol until yellow precipitate was acquired. The mixture was kept at 0 ^oC for overnight. The yellow precipitate is isolated from the overlying reddish-yellow solution with suction filtration and washed with cold methanol.

The yellow solid was further purified for future reactions to remove any reminant

unreacted sodium nitroprusside or by-products [50]. It was recrystallized using an ammonium hydroxide/methanol solution. 30 grams of the yellow sample was dissolved in warm ammonium hydroxide solution (ca. 150 mL) under constant stirring. To this homogenous solution, a cold methanol was added slowly under mild stirring until yellow precipitate was obtained. This bright yellow solid was collected by filtration and rinsed with cold methanol. It was dried by keeping in vacuum desiccator at room temperature for one week. The purification process was repeated for 3 times. The final yield was 50 %.

Due to its highly hygroscopic chararacteristic, it was covered in a closed flask till it was used as precursor for the synthesis of pentacyanoferrate coordinated P4VP metallopolymer.

2.1.2. Synthesis of pentacyanoferrate coordinated poly(4-vinylpyridine)

A synthesis procedure was followed using a known reference [51]. P4VP (200 mg) was dissolved in 50 mL of methanol at room temperature. Because of the limited solubility of sodium aminopentacyanoferrate complex in methanol, excess amount of the sample (600 mg) was added into the solution under constant stirring. After apprx. 15 minutes, the color of the suspension changed from yellow to orange. The reaction was allowed to continue in a covered flask for 3 days. After that, centrifugation at 6000 rpm was done to precipitate the more-dense pentacyanoferrate coordinated P4VP from the suspension. The green precipitate was washed with methanol followed by centrifugation to assure that none of the unlinked pentacyanoamino complex remained in the suspension. The purification process was repeated for 5 times. Finally, 250 mL of cold Et_2O was added into the green $Fe(CN)_5$-P4VP suspension (approximately 50 mL) under stirring. The

brown precipitate was isolated and dried under vacuum overnight at room temperature resulting in a yellowish green powder.

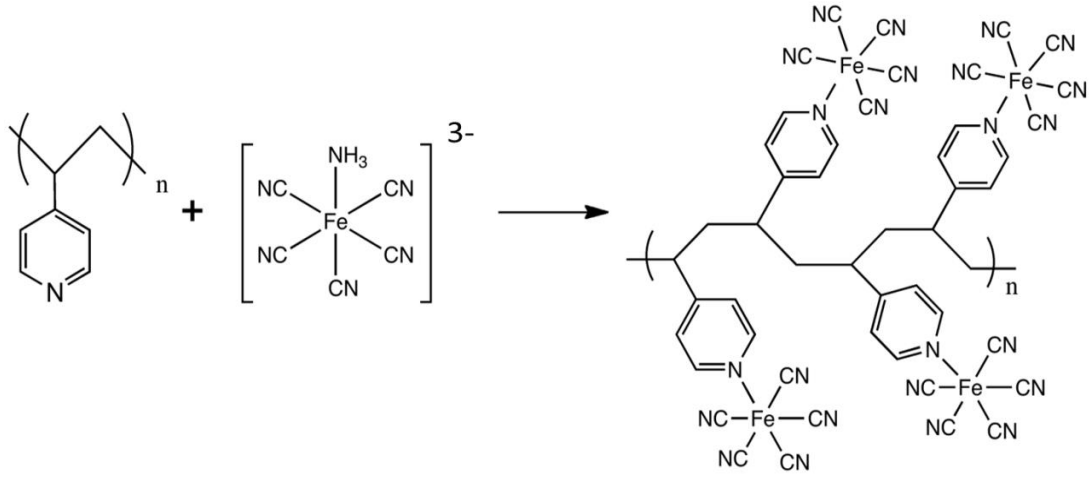

Figure 2.1. Schematic representation of the P4VP coordinated pentacyanoferrate complexes.

2.1.3. Synthesis of Cobalt Pentacyanoferrate coordinated P4VP

50 mL of 10 mM $[Fe(CN)_5\text{-}P4VP]^{3-}$ solution was prepared at room tempretaure. 50 mL of 15 mM $Co(NO_3)_2$ solution was added dropwise under constant stirring. The color of the solution turned to dark green. The resulting dark green solution was left under stirring for 1 hour at room temperature. Afterwards, 100 mL of acetone was added into the solution and the suspension was centrifugated at 6000 rpm for 15 min to collect the solid. The collected solid was washed with 1:1 v/v acetone/water solvent mixture to remove free ions. The purificaton process was repeated for 3 times. The target was collected with the addition of pure acetone and dried in oven at 35 ^{o}C for 1 day.

2.1.4. Synthesis of Cobalt Hexacyanoferrate

Following the drop-by-drop procedure [52], 50 mL of 10 mM $[Fe(CN)_6]^{4-}$ solution was prepared at room tempretaure. 50 mL of 20 mM $Co(NO_3)_2$ solution was added dropwise under constant stirring. The color of the solution turned to bright green. The resulting bright green solution was left under stirring for 1 hour at room temperature. Afterwards, 100 mL of acetone was added into the solution and the suspension was centrifugated at 6000 rpm for 15 min to collect the solid. The collected solid was washed with 1:1 v/v acetone/water solvent mixture to remove soluble unreacted species. The purificaton process was repeated for 3 times. The target was collected with addition of pure acetone and dried in oven at 35 ^{o}C for 1 day.

2.2. *In-situ* Synthesis of Catalyst on the Electrode Surface

Two-step spin coating method is a novel synthetic approach for the preparation of Co-Fe PB coordination compounds. FTO coated glass slide, functionalized by coating with a layer of conductive Flourine doped Tin Oxide film, was used as a substrate for coating purpose. They have 7 Ω/sq surface resistivity, 2 mm thickness and 80-82% transmittance values.

The 2x2.5 cm FTO glass slides were cleaned by following a specific procedure. They were sonicated for 15 minutes in soapy water, distilled water, and isopropanol progressively. Afterwards, they were annealed at 400 °C to improve hydrophilicity by removing the water on the surface and were left to remain under vacuum until coating.

Hydrophilicity of the substrate is a requirement to achieve a flat and homogenous

film on it. Only the 2x1.5 cm part of the FTO slide was coated with Co-Fe PB analogues by using a spin coater and remaining part was masked with a polymeric band.

2.2.1. Preparation of Cobalt Pentacyanoferrate coordinated P4VP on an FTO slide

The $[Fe(CN)_5\text{-}P4VP]^{3-}$ solution containing 0.1 M Fe^{2+} ions was prepared by dissolving 100 mg of the sample in 2 mL of water. The known amount of $[Fe(CN)_5\text{-}P4VP]^{3-}$ solution, 150 µL for 2x1.5 cm, was dropped with a pipette onto a FTO slide and spin coating was done at 1500 rpm for 5 min. Since the excess amount of the solution was ejected off the edges of the slide, the edges of slides were cleaned using distilled water after each coating process. The deposited uniform thin film on FTO has a color of pale yellow. The coated slide was dipped into a 0.15 M Co^{2+} solution horizontally for 15 min to allow Co^{2+} ions to bind to $Fe(CN)_5$-P4VP surface. Then, the slide was washed with distilled water to remove the excess Co^{2+} ion over the film. The color of deposited film changed from yellow to bright green as a result of the chemical reaction between $[Fe(CN)_5\text{-}P4VP]^{3-}$ and Co^{2+} ions. The same procedure was repeated for 5 times.

2.2.2. Preparation of Cobalt Hexacyanoferrate on an FTO slide

The same procedure was applied for the preparation of Cobalt Hexacyanoferrate modified FTO electrode with a slight difference. In this case, the molar ratio of the prepared $[Fe(CN)_6]^{4-}$ solution to Co^{2+} was 2:1 due to charge balance although

it is 3:2 for the preparation of $CoFe(CN)_5$-P4VP. When the spin coated slide was dipped into the Co^{2+} solution, the color turned to pale green (Figure 2.2).

All of the coated FTO slides were kept under vacuum overnight prior to use.

Figure 2.2. The photo of FTO coated $CoFe(CN)_6$ sample before electrochemical analysis.

2.3. Instrumentation

2.3.1. Fourier Transform Infrared Spectroscopy (FTIR)

FT-IR analysis was carried out to record the transmission spectra of each powder and FTO coated sample, which has a characteristic absorption frequency, especially in the 2000-2200 cm^{-1} region for cyano compounds. For the FTO coated samples, the sample was collected by peeling off from the surface of FTO slides. The spectra were obtained by Bruker ALPHA Platinum-ATR Spectrometer in the mid-IR range 4000–400 cm^{-1} at room temperature.

2.3.2. UV-Visible Spectroscopy (UV-Vis)

The UV-Vis absorption spectra were recorded by using Cary 300 UV-Vis Spectrometer in the 400-700 nm region with a scan rate of 600 nm/min.

2.3.3. X-Ray Diffraction (XRD) Patterns

X-ray diffraction studies were performed to investigate the crystalline behavior of all of the synthesized materials. X-Ray diffraction patterns of powder samples were recorded by PANalytical's X'Pert Powder X-ray diffractometer (Multiple Purpose Diffractometer) by employing CuKα X-ray radiation (λ=1.5418 Å) in the diffraction angle (2θ) 10-70° range with a step size of 0.01 and a scan rate of 1° min^{-1}.

2.3.4. Scanning Electron Microscopy (SEM) and Energy Disperse X-Ray Analysis (EDX)

Scanning electron microscopy (SEM) imaging and Energy-dispersive X-ray spectroscopy (EDX) analysis was carried out using FEI-Quanta 200 FEG ESEM operated with the resolution of 1.5 nm at 30kV. Based on the EDX analysis data, the elemental composition of the samples (Fe, Co, and K) was identified. For each analysis, multiple points were recorded and the mean value was reported.

2.3.5. X-Ray Photoelectron Spectroscopy (XPS)

Thermo scientific K-α X-ray photoelectron spectrometer (XPS) system operating along with micro-focused monochromated Al Kα X-ray source gun and a flood gun for charge neutralization was employed to record the spectra with data acquisition parameters of 1486.6 eV source energy, 400 μm spot size, 30.0 eV

pass energy, 0.100 eV energy step size.

2.3.6. CHNS/O (Elemental) Analysis

Elemental analysis data was acquired by Thermo Scientific FLASH 2000 CHNS/O Analyzer. With combination of both CHN and EDX data, the molecular formulas of the compounds were estimated.

2.3.7. Electrochemical Measurements

The electrochemical experiments were carried out at room temperature by using Gamry Instruments Interface 1000 Potentiostat with a two-compartment electrochemical cell using three electrodes. The modified FTO was the anodic working electrode since the main oxidation reaction was performed on it. As the counter electrode, Pt wire was employed to balance the reaction occurring on the working electrode. It was isolated from the main solution by using a glass frit to prevent the solution from conatining any kind of by-product, which might be produced on the counter electrode. Ag/AgCl (3.5 M KCl) served as a reference electrode and all of the potential values were explained versus Ag/AgCl reference electrode. 50 mM potassium phosphate buffer solution (at pH=7) involving 1 M KNO_3 was prepared to be used as electrolyte and to maintain the pH of the medium constant.

All three electrodes were dipped into the buffer solution including electrolyte that was bubbled using N_2 gas for 15 mins to remove the dissolved O_2 gas before each measurement. Along the measurement, the system was closed.

All cyclic voltammetry and chronoamperometry measurements were carried out by following the procedure explained above.

2.3.8. Bulk Water Electrolysis

Oxygen evolution in bulk-water electrolysis was determined with a YSI 5100 Oxygen-sensing instrument equipped with a dissolved oxygen field probe. The oxygen probe was inserted into the anodic part of two-compartment gas-tight electrochemical cell with a glass frit separation. The coated FTO electrode as working electrode, Pt wire as a counter electrode and Ag/AgCl as reference electrode were placed into the respective compartments and the experiments were carried out in KPi buffer (pH = 7) solution containing 1 M KNO_3.

The bulk electrolysis was performed at 1.2 V vs. Ag/AgCl for 3 hours. The amount of dissolved O_2 molecules was detected to compare with the theoretical amount of evolved O_2 assuming a Faradaic efficiency of 100% .

Origin Pro 8.5 software was used to plot all the graphs and analyze the data obtained.

Chapter 3

RESULTS AND DISCUSSION

3.1. Characterization of Catalysts

The characterization results of the all prepared samples were reported in this part. In the light of well-known pentacyano and hexacyano chemistry, it was assured that the obtained samples possess all the requirements of promising PB type compounds. The electrochemical activities of the prepared electrodes was tested and compared with the similar literature.

3.1.1. Infrared Studies

The ATR spectra of both $Fe(CN)_5NH_3$ and $Fe(CN)_5$-P4VP complexes were studied to confirm the binding of pentacyanoferrate to pyridyl moieties of the P4VP by comparison of both analysis (Figure 3.1). The most significant part of this investigation was based on the CN stretching mode, which generally exhibits a strong, sharp, and intense absorption peak in the 2200-2000 cm^{-1} range [53]. Due to the similar π-accepting capability of pyridine and CN ligand, there will be less π-back donation of iron to antibonding orbital of CN groups (t_{2g} (Iron)→ π^* (Pyridine)) for $Fe(CN)_5$-P4VP complex. This results in the increment in C-N bond frequency, which is blue shifted from the CN stretching band, in the amino pentacyanoferrate complex [54].

The cyanide stretch, bound to Fe^{II}, was observed at 2041 cm^{-1} for the prepared $Fe(CN)_5$-P4VP complex with an 8 cm^{-1} blue shift, suggesting that the target

metallopolymer was obtained. Furthermore, a less intense peak referring to stretching of CN ligand connected to Fe^{III} was observed at 2112 cm^{-1}, which indicates the partial oxidation of the pentacyano ferrate complex [54].

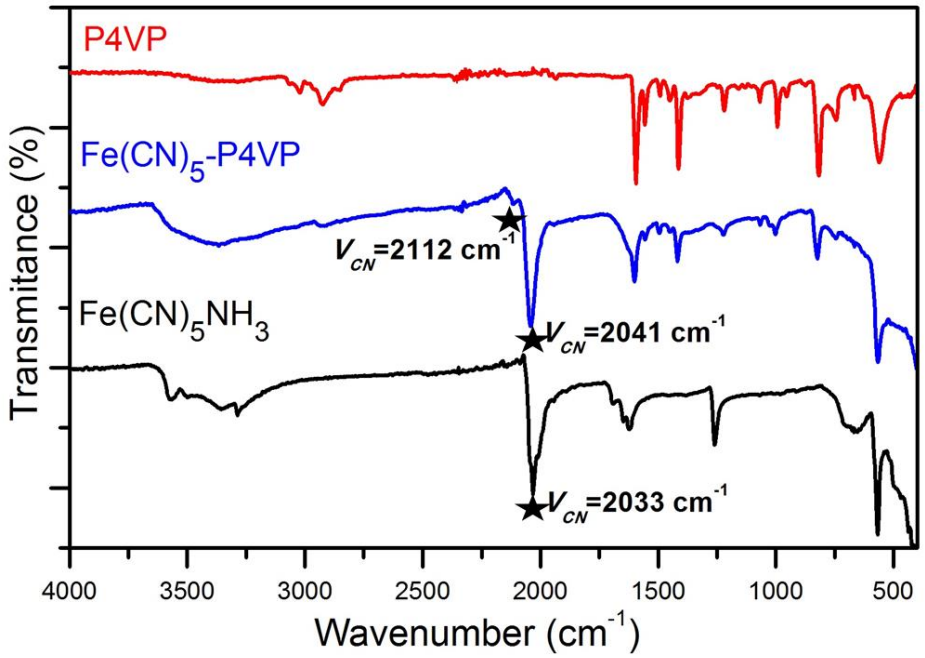

Figure 3.1. The FTIR Spectra of $Fe(CN)_5NH_3$, $Fe(CN)_5$-P4VP, and P4VP.

The $\nu(CC_{ring})$ and $\nu(CN_{ring})$ bands of pyridine group were also investigated to verify the coordination of pentacyanoferrate groups to P4VP (Figure 3.2). The $\nu(CN_{ring})$ band at 1595 cm^{-1} of pure P4VP shifts to 1600 cm^{-1} for $Fe(CN)_5$-P4VP. The same trend was also noted for the $\nu(CC_{ring})$ band at 1413 cm^{-1} that shifts to 1417 cm^{-1}. The observed stretching band values for each mode are in close similarity with the literature. The observation of the blue shift is the proof of complexation between pentacyanoferrate and pyridine moities of P4VP [55, 56].

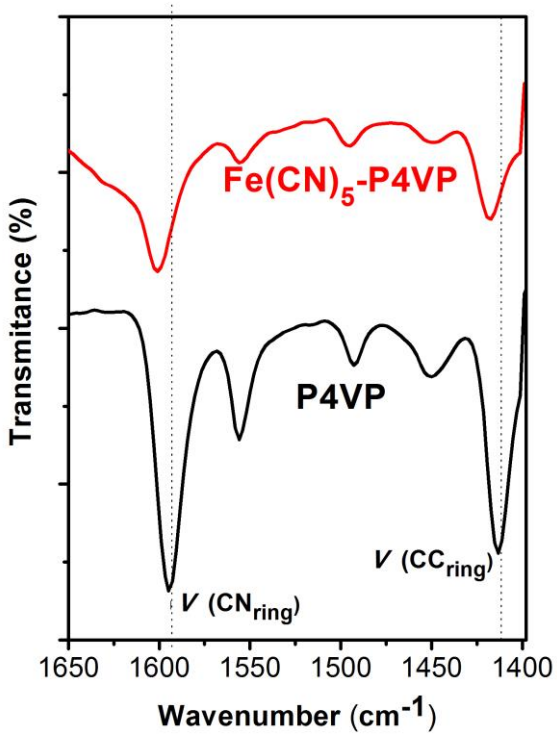

Figure 3.2. The FTIR Spectra of P4VP and $Fe(CN)_5$-P4VP.

The CN stretch band undergoes a pronounced blue shift after inclusion of Co^{2+} ions to the metallopolymer to obtain PB stucture (Figure 3.3). The cyanide band for each sample represents the linear bridging Fe-CN-Co binding mode [57].

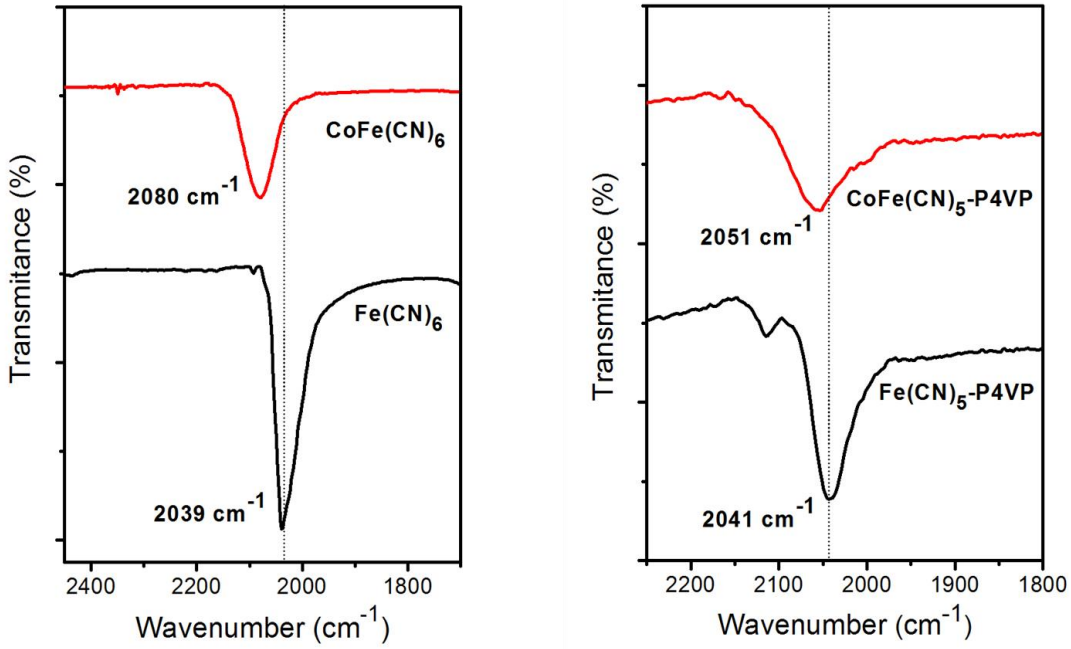

Figure 3.3. The FTIR Spectra of $Fe(CN)_6$ and $Fe(CN)_5$-P4VP before and after addition of Co^{2+}.

3.1.2. UV-Vis Absorption Studies

The pentacyanoferrate complexes, $[Fe(CN)_5L]^{3-}$, have characteristic charge transfer absorption in the visible light range that is related to σ-donor and π-acceptor capability of the sixth ligand. The O_h symmetry of the $[Fe(CN)_6]^{4-}$ ion is lowered to C_{4v} local symmetry with the substitution of cyanide group with ligand L. The number of vibrational modes for C_{4v} symmetry is 15 according to the 3N-6 rule and all vibrational modes are $4A_1$, $2B_1$, B_2 and 4E. Within all modes, the infrared active ones are E, A_2, and A_1 that are totally symmetric. A transition from the ground state $^1A_1$ to excited state ^1E is the only spin allowed d-d transition with the highest molar absorptivity coefficient and it is sensitive to the nature of L [39].

The UV-Vis spectra of both amino pentacyanoferrate and P4VP-coordinated pentacyanoferrate were studied to observe any shift in the absorption band due to the substitution of the sixth ligand (Figure 3.4). The UV-Vis absorption band was observed at 404 nm for the preliminary synthesized amino pentacyanoferrate, which is consistent with the literature. The UV-Vis absorption peak shifts to higher energy, located at 378 nm, for P4VP coordinated pentacyanoferrate due to MLCT transition from d orbital of iron to π-antibonding orbital of pyridine moieties, which shows a similar UV-Vis absorption feature of the desired metallopolymer [58].

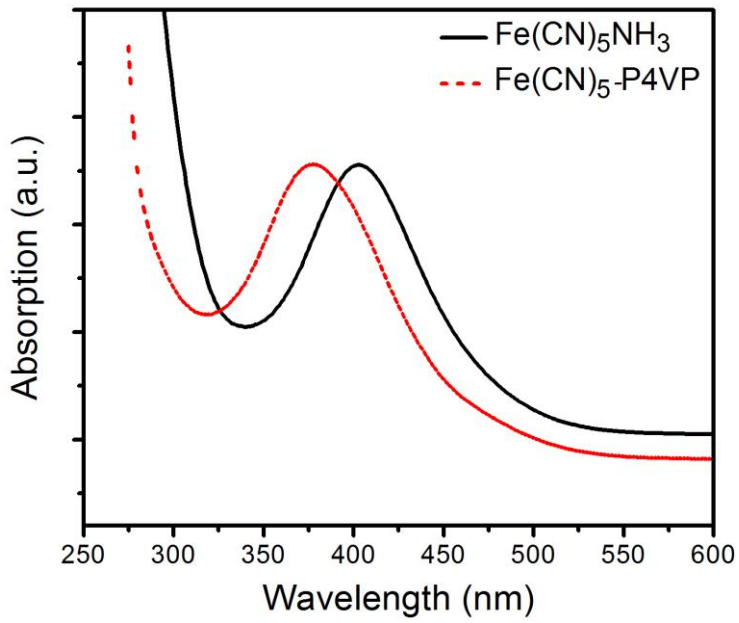

Figure 3.4. The UV-Vis Spectra of $Fe(CN)_5NH_3$ and $Fe(CN)_5$-P4VP.

3.1.3. Elemental Analysis

It was done to find out the chemical formula of the prepared samples by using Molecular Weight Calculator Software. The CHN and XPS analyses were performed

and compared with the theoretical values. The results are represented in the table (Table 3.1).

Table 3.1. Weight percent value of each element in the $Fe(CN)_5NH_3$ complex.

$Na_3(Fe(CN)_5NH_3)(H_2O)_3$	C	H	N	Fe*	Na*
MW = 325.97791	%	%	%	%	%
Theoretical	18.42	2.783	25.78	17.13	21.16
Experimental	18.96	3.001	25.34	17.15	20.88

*EDX results

The experimental and theoretical data are in good aggrement with each other.

The Fe content of the $Fe(CN)_5$-P4VP sample was investigated with the help of EDX. For this purpose, 10 different points on the sample were chosen to get more precise results for Fe content. All results were in good agreement with the expected formula that proves the homogenity of the sample. The results were listed in the Table 3.2.

Table 3.2. Atomic and weight percent ratio of Fe & Na elements in $Fe(CN)_5$-P4VP metallopolymer.

# of EDX Analysis	Fe content w/w%	Na content w/w%	Fe content Atom %	Na content Atom %
1	12.24	14.58	3.48	10.07
2	11.86	14.20	3.35	9.75
3	12.75	14.44	3.65	10.04

4	12.71	14.70	3.63	10.20
5	11.99	14.12	3.40	9.72
6	11.06	15.44	3.11	10.55
7	11.75	15.66	3.34	10.81
8	11.52	15.30	3.27	10.56
9	10.92	15.63	3.10	10.79
10	10.48	15.03	2.95	10.27
Average Number	**11.73**	**14.91**	**3.328**	**10.28**

According to this result, the atomic ratio of Na to Fe is equal to ~3, which is the same ratio observed in the amino pentacyanoferrate complex. It can be concluded that the oxidation state of Fe^{2+} ion remains the same to a sufficient extent. The weight percent of both Fe and Co were shown in the Table 3.2. The CHN analysis was performed that yields C 36.43, H 3.387, N 18.83 w/w%. By combining both EDX and CHN analysis data, the weight percent of pyridyl groups in the polymer that coordinate to pentacyanoferrate ions was calculated. 74.12% of pyridyl moities of polymer were coordinated to the pentacyanoferrate based on the Fe/C weight percent ratio.

EDX analysis was also carried out for $CoFe(CN)_6$ and $CoFe(CN)_5$-P4VP bulk samples. It was confirmed that freshly prepared $CoFe(CN)_5$-P4VP sample has an atomic ratio of 1:1.45 of Fe to Co (Figure 3.5) with traces of Na, which closely corresponds with the theoretical ratio (1:1.5). The result indicates that coordination compound has an empirical formula of $Co_{1.5}$[Fe(CN)$_5$PVP].xH2O.

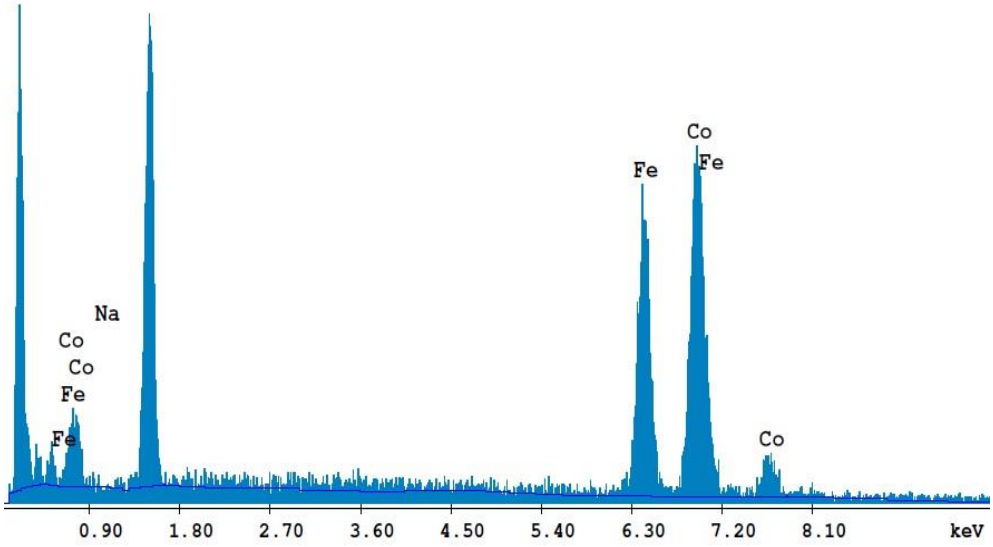

Figure 3.5. EDX spectrum of the $CoFe(CN)_5$-P4VP.

Whereas, for $CoFe(CN)_6$, the ratio is found to be 1:1.65, with moderate amount of K, indicating the resulting coordination compound to have an empirical formula of $K_{0.7}Co_{1.65}[Fe(CN)_6].xH2O$ (Figure 3.6).

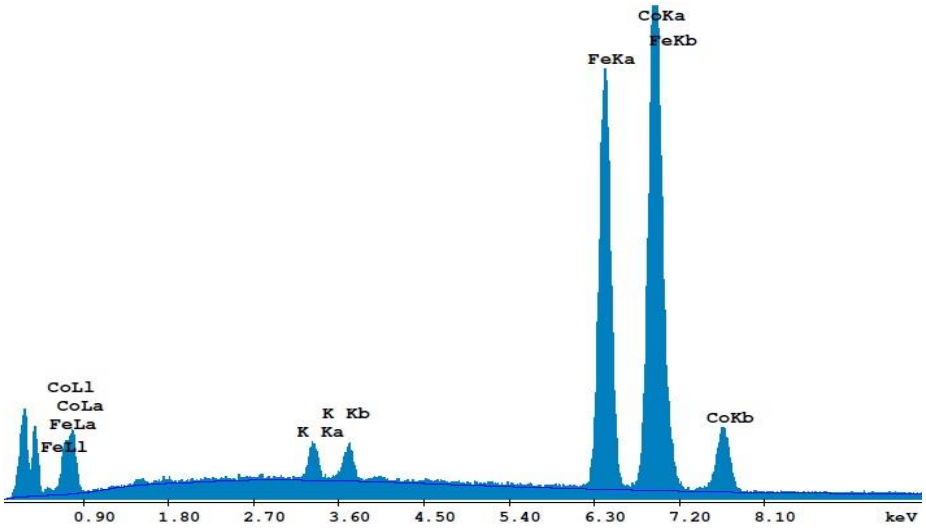

Figure 3.6. EDX spectrum of the $CoFe(CN)_6$.

3.1.4. Powder X-Ray Diffraction Studies

The compounds were characterized by X-ray diffraction technique reflecting the patterns identical to highly symmetric Fm3m (face centered cubic structure) space group that belongs to Prussian blue analogues.

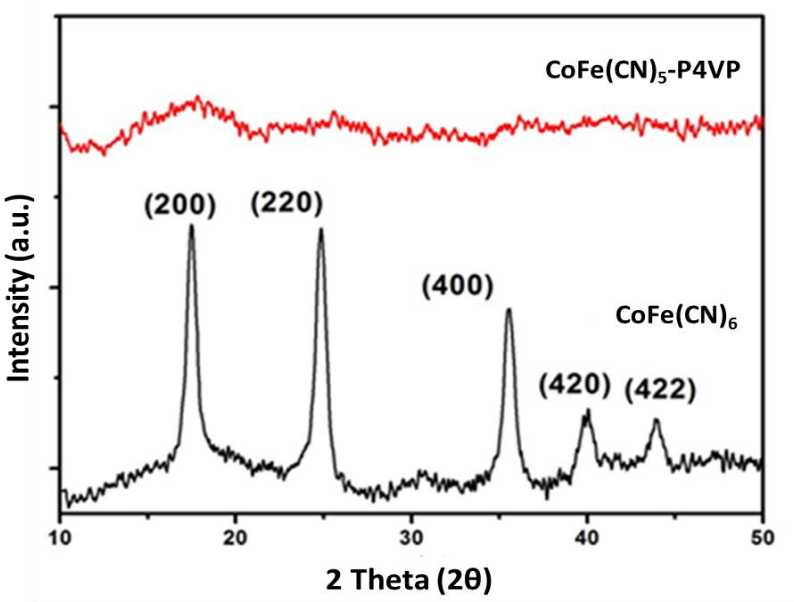

Figure 3.7. XRD pattern of $CoFe(CN)_6$ and $CoFe(CN)_5$-P4VP.

The X-ray powder diffraction pattern for $CoFe(CN)_6$ represents very intense, sharp peaks with indices 200, 220, 400, 420, and 422 at the corresponding diffraction angles [59] while the one for $CoFe(CN)_5$-P4VP exhibits much broad features due to amorphous nature of the compound (Figure 3.7).

3.2. Characterization of the Pristine Co-Fe PB coated FTO Electrodes

Both $CoFe(CN)_6$ and $CoFe(CN)_5$-P4VP coated FTO electrodes were investigated by applying FTIR, XPS, XRD, SEM and EDX techniques. The results obtained from bulk samples have been used as reference for comparison. The corresponding IR spectra for each sample grown on FTO electrode were represented in the graph below (Figure 3.8).

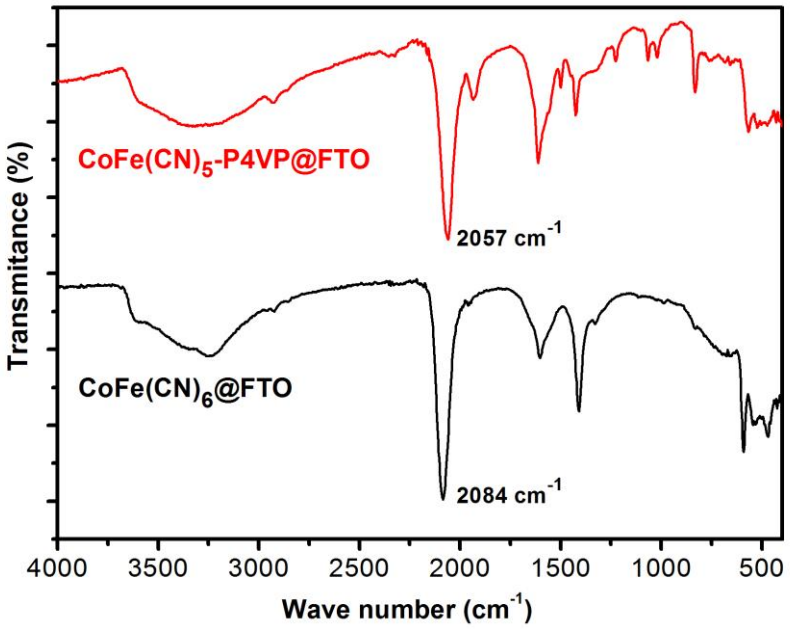

Figure 3.8. The FTIR spectra of pristine CoFe PB coated on FTO.

The band corresponding to CN stretch at 2041 cm^{-1} for $Fe(CN)_5$-P4VP (Figure 3.1) showed a blue shift to 2057 cm^{-1} for FTO growth $CoFe(CN)_5$-P4VP, which is characteristic of Fe^{II}-CN-Co^{II} binding mode [57]. The same band value for the bulk $CoFe(CN)_5$-P4VP is observed at 2051 cm^{-1}, which corresponds well with the FTO coated one. For the $CoFe(CN)_6$ sample, the CN stretching band for FTO coated is 2084 cm^{-1}, which is in good agreement with bulk one at 2080 cm^{-1}.

XPS analysis for pristine FTO coated samples was carried out to investigate the oxidation state of the active metal sites (Figure 3.9). For both CoFe samples, the oxidation state of cobalt is expected to be +2, which is proven by Infrared studies. $Co(NO_3)_2.6H_2O$ and $K_3[Co(CN)_6]$ were used as reference compounds for Co^{II} and Co^{III} so that a suggestion on the oxidation state of pristine samples can be made accurately. As shown in the graph, the peaks get sharper and well-defined when the oxidation

number increases from +2 to +3 and the satellite peaks associated with each principle line starts to disappear. Furthermore, each of the principle lines exhibit a strong band with a scalable FWHM value (>3.5 eV) and they are suitable for identification. However, satellite peaks associated to $Co2p_{1/2}$ and $Co2p_{3/2}$ are broad and not suitable for identification [60].

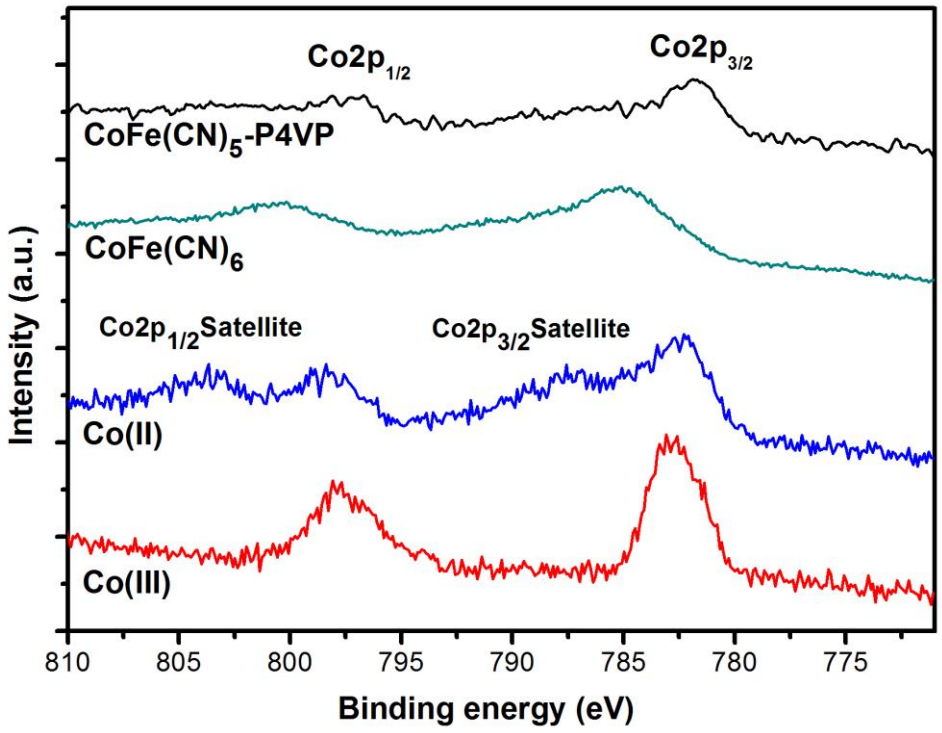

Figure 3.9. XPS spectra of pristine $CoFe(CN)_6$@FTO and $CoFe(CN)_5$-P4VP@FTO.

For the $CoFe(CN)_5$-P4VP on FTO, the $Co2p_{3/2}$ line at 781.88 eV with a strong satellite band, which is 4-8 eV above the principle band is observed. Additionally, the $Co2p_{1/2}$ line positioned at 796.68 eV with a satellite peak that is 5-6 eV above the principal line is also recorded. The observed peak values are in a good agreement with the Co(II) salt, which exhibits $Co2p_{3/2}$ line at 782.28 eV and $Co2p_{1/2}$ line at 798.38 eV [61, 62].

The $CoFe(CN)_6$ on FTO sample with $Co2p_{3/2}$ line positioned at 784.68 and $Co2p_{1/2}$ line at 800.48 eV shows slight shift from the reference Co(II) salt, however the peak values are still in a safe range with a predominant satellite band.

XRD analysis of both $CoFe(CN)_6$ and $CoFe(CN)_5$-P4VP samples on FTO (Figure 3.10) was carried out. The peaks that belong to blank FTO glass was labeled with marks (*). The remaining peaks representing the typical pattern of Prussian Blue structure (▲) were only observed for $CoFe(CN)_6$, as is the case of bulk samples [59].

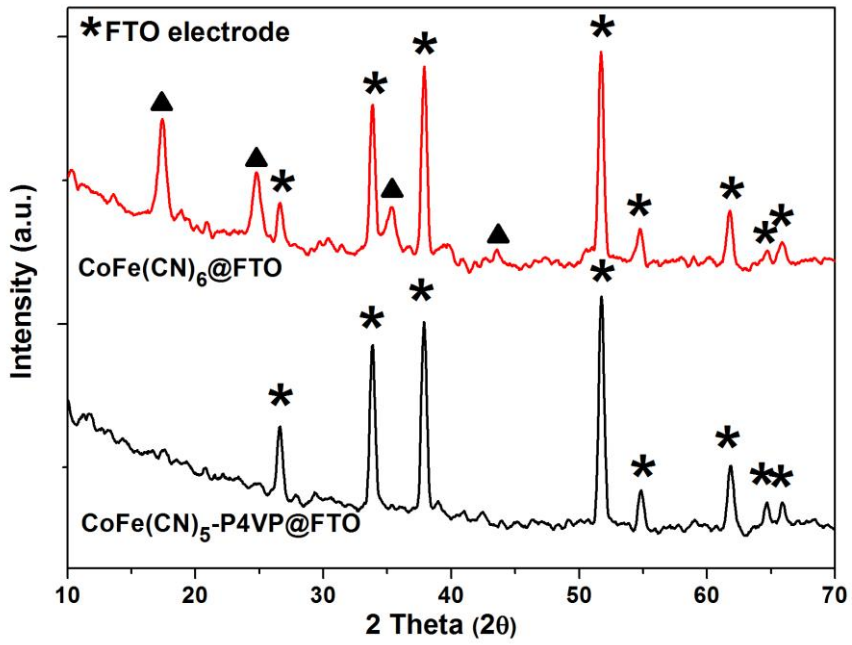

Figure 3.10. Powder X-ray diffraction patterns of $CoFe(CN)_6$@FTO and $CoFe(CN)_5$-P4VP@FTO.

SEM imaging was performed for the $CoFe(CN)_5$-P4VP sample coated on FTO to investigate the morphology of the electrode (Figure 3.11). The image suggests that the coating is consistent with no long term orderliness,which also explains the amorphous

nature of the catalyst. The coating exhibits sub-micron sized catalyst particles distributed uniformly all over the electrode surface.

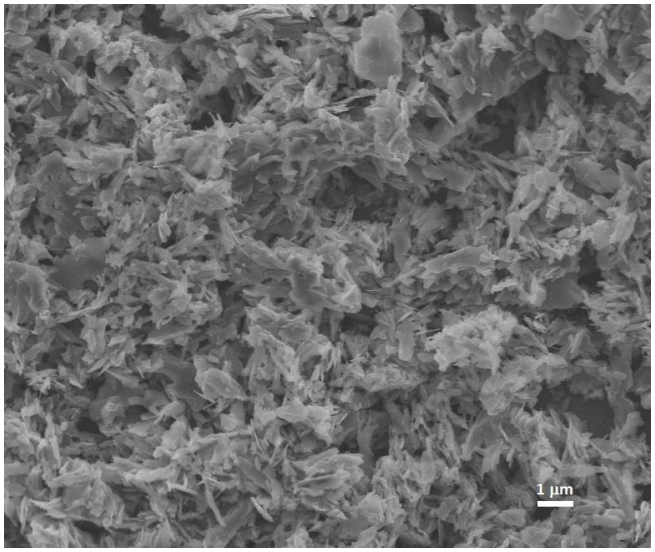

Figure 3.11. SEM image of $CoFe(CN)_5$-P4VP@FTO electrode.

To study the Fe to Co ratio of the catalysts on the FTO electrodes, EDX analysis was performed to compare the results with the results mentioned in Section 3.3. To avoid the high intensity signals of Tin (Sn) and florine (F), the coatings were carefully peeled off from the electrode and then the EDX analysis was performed. The EDX analysis performed on the prisitine $CoFe(CN)_5$-P4VP catalyst confirmed an atomic ratio of 1:1.42 of Fe to Co, with traces of Na (Figure 3.12), which closely corresponds with the ratio for the freshly prepared bulk $CoFe(CN)_5$-P4VP catalyst (1:1.45).

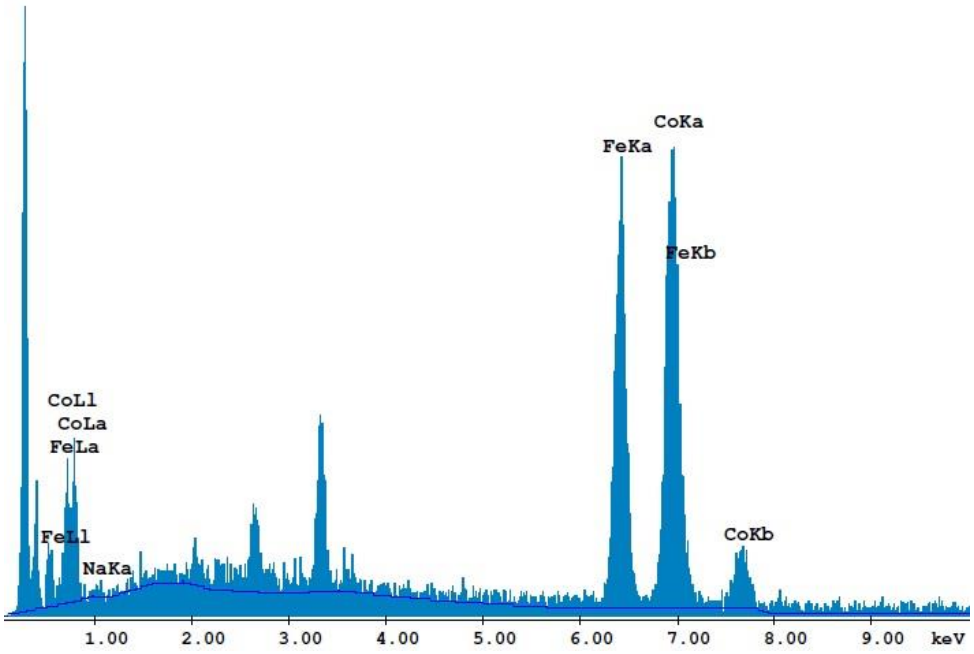

Figure 3.12. EDX spectrum of the pristine $CoFe(CN)_5$-P4VP@FTO sample.

The pristine $CoFe(CN)_6$ catalyst peeled off from the FTO confirmed a ratio of 1:1.66, with moderate amount of K (Figure 3.13), which is in good accordance with the ratio of freshly prepared bulk $CoFe(CN)_6$ catalyst (1:1.65).

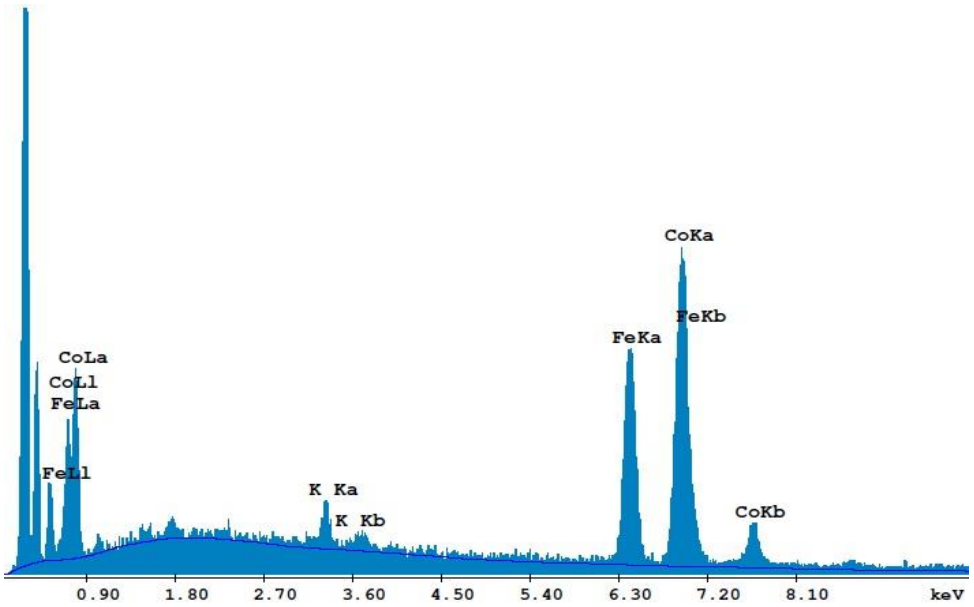

Figure 3.13. EDX spectrum of the pristine $CoFe(CN)_6$@FTO sample.

3.3. Electrochemical Water Oxidation Studies of Co-Fe PB coated FTO Electrodes

3.3.1. Cylic Voltammetry Measurements for $CoFe(CN)_5$-P4VP on FTO

Cyclic voltammogram of $CoFe(CN)_5$-P4VP deposited on FTO was recorded in the -0.4 - 1.8 V range with respect to Ag/AgCl reference electrode. A quasi-reversible redox couple with an oxidation peak at 0.46 V and a reduction peak at 0.26 V vs NHE ($E_{1/2}$ = 0.36 V, Ec − Ea = 200 mV) was observed (Figure 3.14). This one electron process can be attributed to Co^{II} Fe^{II} /Co^{III} Fe^{II} redox couple [63]. An irreversible peak, appeared above 1.1 V, corresponds to catalytic water oxidation process.

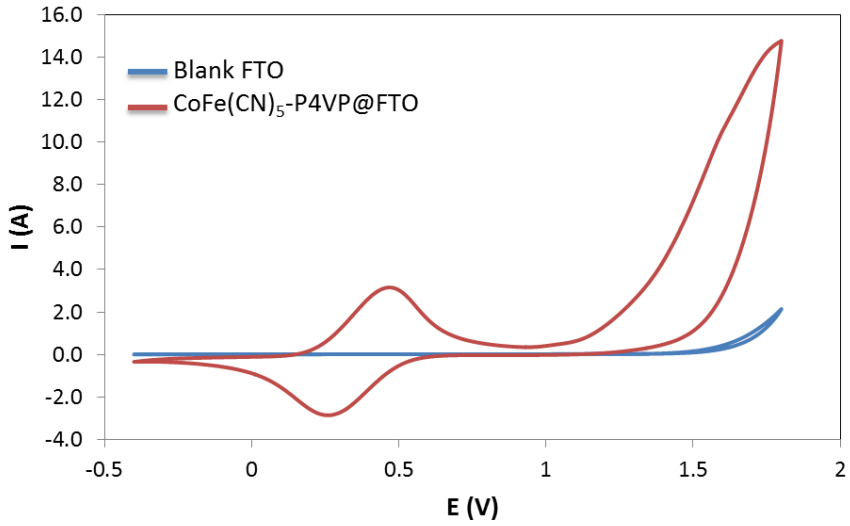

Figure 3.14. Cyclic voltammogram of $CoFe(CN)_5$-P4VP on FTO electrode recorded in 50 mM KPi electrolyte at pH = 7.0 (red line) with a 25 mV/s sweep rate. Electrochemical response of blank FTO electrode (blue line).

The Co^{II} Fe^{II} /$Co^{III}Fe^{II}$ redox pair was evaluated to determine the surface concentration of active cobalt sites on the electrode. For this reason, the cyclic voltammogram in -0.4 - 1.4 V potential range was recorded with different scan rates (between 25-500

mV/sec) (Figure 3.15, Left). The reduction peak current *I* (mA) versus scan rate *v* (mV/sec) was plotted (Figure 3.15., Right). In the graph, the linearity was observed between 200 to 450 mV/sec scan rate. By using the slope of the linear trendline, the active Co concentration of the surface was calculated according to equation 3.1 below.

$$slope = \frac{n^2 F^2 A \Gamma}{4RT} \qquad \text{(Eq. 3.1)}$$

in which n =1 (1 e^- redox process), F= Faraday's constant, A= Surface Area, Γ = Surface concentration (mol/cm^2), R= ideal gas constant, and T= Temperature [64].

Surface concentration of redox active cobalt centers on $CoFe(CN)_5$-P4VP on FTO is calculated as 13.8 nmol.cm^{-2}.

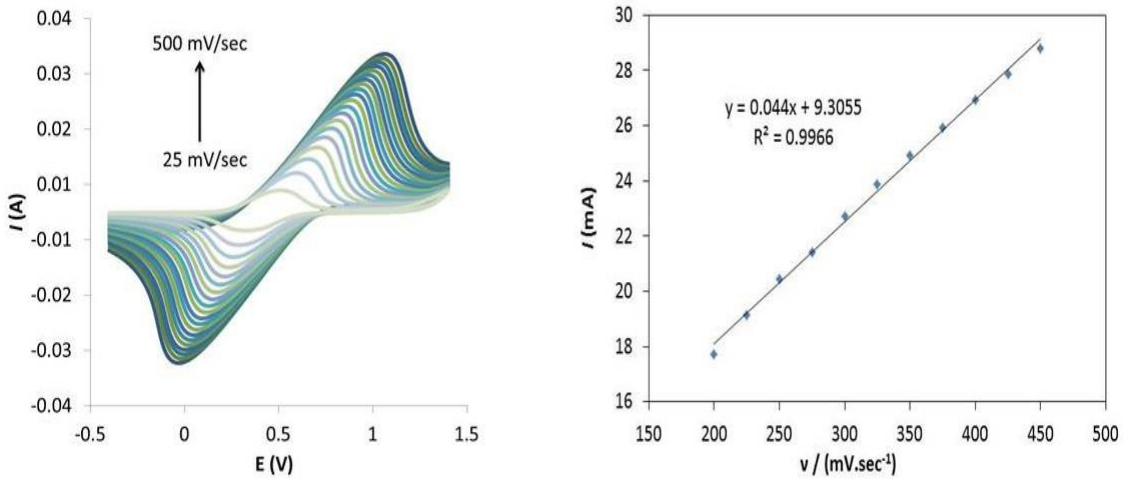

Figure 3.15. Cyclic voltammograms of $CoFe(CN)_5$-P4VP on FTO electrode in 50 mM KPi buffer solution at pH = 7 recorded at different scan rates, υ (Left). The linear relation between the reverse peak current of $Co^{2+/3+}$ redox couple and the scan rate between 200 to 450 mV/sec scan rate (Right).

3.3.2. Cylic Voltammetry Measurements for $CoFe(CN)_6$ on FTO

For the comparison of surface concentration on $CoFe(CN)_6$ electrode with $CoFe(CN)_5$-P4VP electrode, the cyclic voltammograms with different scan rates (between 200-450 mV/sec) in 0-1.4 V potential range were recorded with respect to Ag/AgCl reference electrode (Figure 3.16).

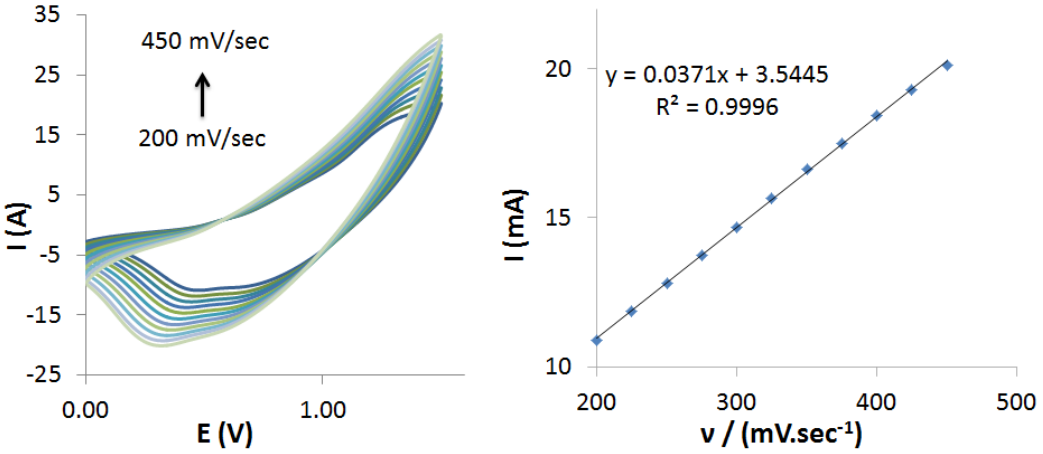

Figure 3.16. Cyclic voltammograms of $CoFe(CN)_6$ on FTO electrode in 50 mM KPi buffer solution at pH = 7 recorded at different scan rates, υ (Left). The linear relation between the reverse peak current of $Co^{2+/3+}$ redox couple and the scan rate between 200 to 450 mV/sec scan rate (Right)**.**

By plugging the slope value obtained from linear region into the equation 3.1, the surface concentration value was calculated as 2 $nmol.cm^{-2}$.

3.3.3. Comparison of the catalytic activity of both CoFe samples

Chronoamperometry measurement was performed at different applied potential along 600 s equilibrium time. The steady current density data was collected for each overpotential to evaluate the catalytic activity of both samples. The Tafel Plot, which

correlates current density and overpotential, was shown in the graph (Figure 3.17). The linearity obtained in intermediate potentials (300-500 mV) with a Tafel slope of 121 mV/decade for $CoFe(CN)_5$-P4VP and 111 mV/decade for $CoFe(CN)_6$ is between the values expected for an electrochemical rate-limiting step observed for such systems [12]. Although a higher Tafel slope is obtained for $CoFe(CN)_5$-P4VP compared to $CoFe(CN)_6$, the current density values show a significant progress. 1 mA/cm^2 of catalytic current density for $CoFe(CN)_5$-P4VP was achieved at η = 510 mV. A catalytic onset potential of 360 mV is required to obtain a current density of 55 $\mu A/cm^{-2}$. Since the oxygen bubbles that limit mass transport on the electrode surface occurs at higher overpotentials, a deviation from linearity is observed (Figure 3.18).

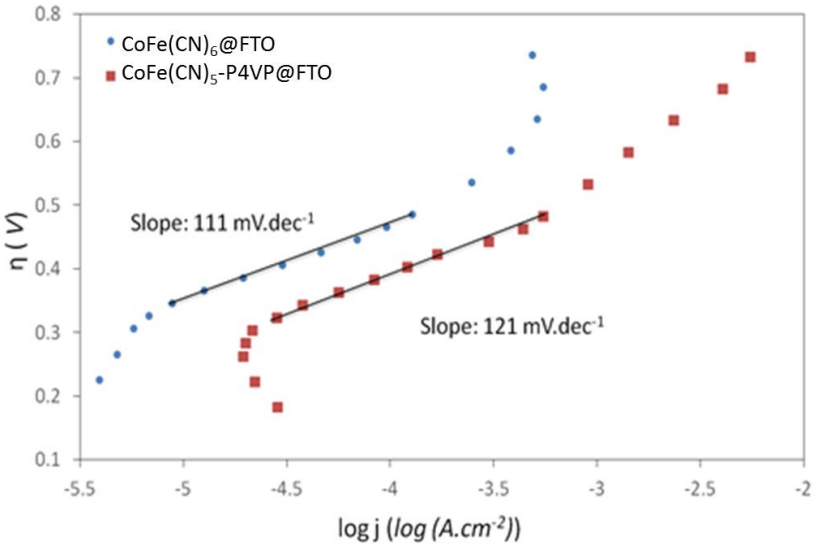

Figure 3.17. Tafel plots for $CoFe(CN)_6$@FTO (blue circles) and $CoFe(CN)_5$-P4VP@FTO (red squares) electrodes from 0.9 to 1.1 V vs. Ag/AgCl electrode recorded in 50 mM KPi electrolyte at pH = 7.0.

By using the surface coverage value, the minimum TOF value can be calculated by following the equation 3.2 below.

$$TOF = \frac{Q}{4t\Gamma} \qquad \text{(Eq. 3.2.)}$$

where Q = integrated charge through the modified FTO electrode ($C.cm^{-2}$), Γ = Surface concentration (mol/cm^2), t = time, and 4 is equal to number of e^-'s required for oxidation of 1 mole of O_2 [65].

Figure 3.18. Evolution of oxygen bubbles on $CoFe(CN)_5$-P4VP modified FTO electrode at an constant potential of 1.2 V.

The reaction occurs only on the surface of the catalyst although all of the material is electrochemically active. So, the surface concentration calculated from the peak current value of Co^{III}/Co^{II} at different scan rates is the upper limit to the number of active sites.

By applying surface coverage number to linear Tafel region, a TOF value of 2.6×10^{-3} s^{-1} could be achieved at overpotentials of 262 mV and 284 mV (Figure 3.19), respectively, for $CoFe(CN)_6$ and $CoFe(CN)_5$-P4VP. The similarity in log TOF vs η plots indicate that active cobalt sites have similar coordination spheres as expected. It

should be noted here that introducing polymeric moiety should not have a significant effect to the coordination sphere of cobalt sites since polymer P4VP is connected to iron center and cobalt site is surrounded by terminal nitrogen atoms of cyanide group in both catalysts.

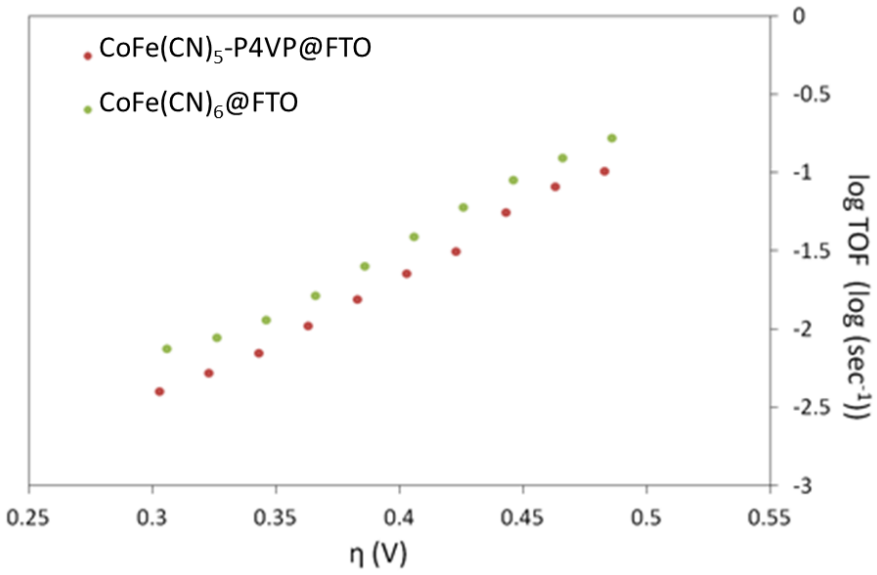

Figure 3.19. Dependence of turnover frequencies of $CoFe(CN)_6$@FTO (green circles) and $CoFe(CN)_5$-P4VP@FTO (red circles) electrodes in the 0.9 to 1.1 V (vs. Ag/AgCl electrode) range recorded in 50 mM KPi electrolyte at pH = 7.0.

3.3.4. Bulk Water Electrolysis of $CoFe(CN)_5$-P4VP modified FTO electrode

The quantity of O_2 produced during bulk electrolysis of $CoFe(CN)_5$-P4VP modified FTO electrode at a constant potential of 1.2V was measured by an oxygen sensing instrument along 3 hours (Figure 3.20.). For comparison, the theoretical amount of evolved O_2 was calculated using Faraday's Law for a $4e^-$ process (assuming a Faradaic efficiency of 100%). The theoretical fit (red line), which matches the experimental slope (black line) for oxygen evolution, clearly shows that the origin of increase in

current is water oxidation catalysis. After two hours, the instrument reached saturation and allowed to continue only for 1 more hour.

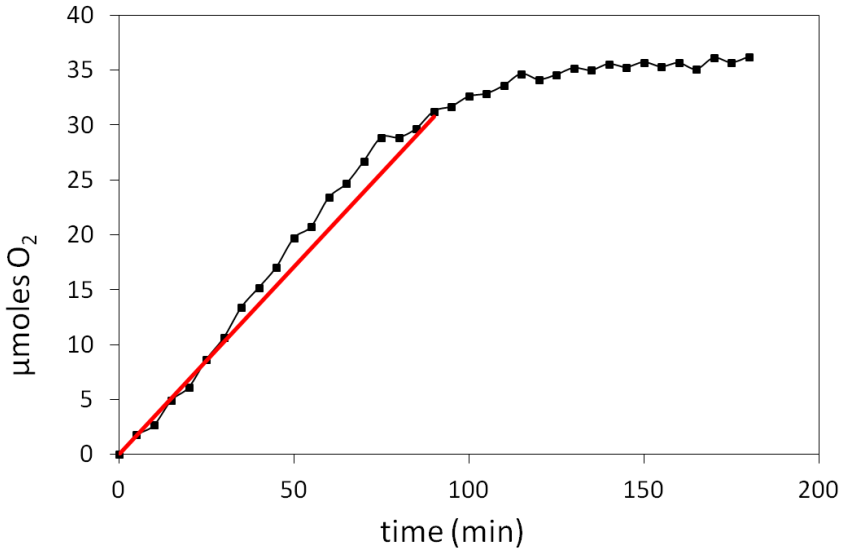

Figure 3.20. Faradic efficiency of $CoFe(CN)_5$-P4VP@FTO measured by an oxygen sensor system.

A stable current was observed that suggests the stability of $CoFe(CN)_5$-P4VP@FTO electrode during electrolysis along three hours (Figure 3.21). A color change from green to orange due to partial oxidation of Co(II) sites to Co(III) was also observed (Figure 3.21., Inset).

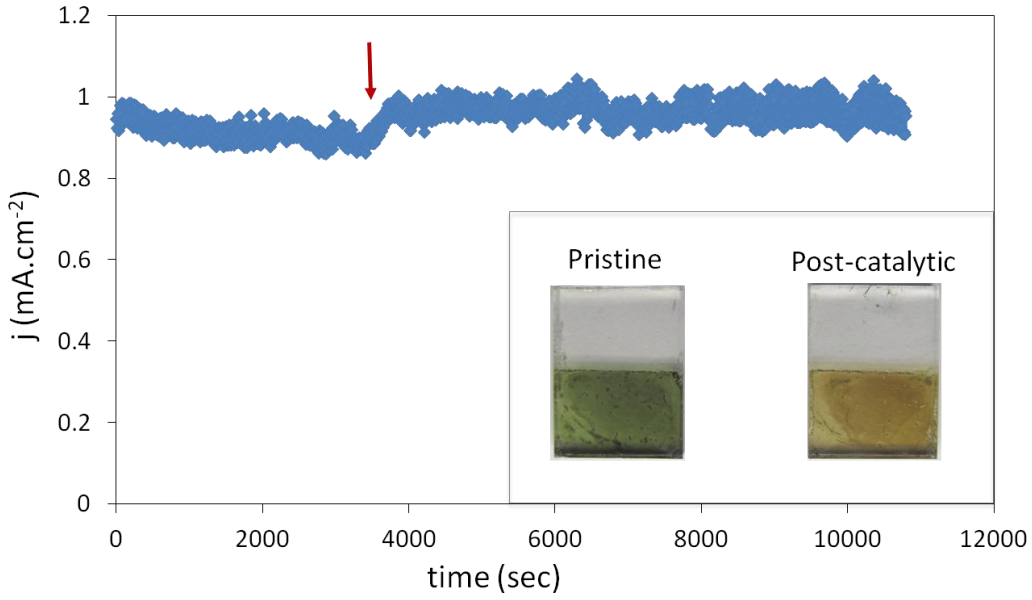

Figure 3.21. Chronoamperometry measurement of $CoFe(CN)_5$-P4VP@FTO electrode at 1.2 V vs. Ag/AgCl in KPi buffer at pH = 7. The red arrow indicates mechanical removal of bubbles. The inset shows the images of electrodes before and after catalytic process.

3.4. Characterization of Post-catalytic Co-Fe coated FTO electrodes

Infrared and XPS studies of pre and post-catalytic samples were performed to investigate the behaviour of partial oxidation as well as the stabilities of electrodes. Post-catalytic samples were treated with a reduction potential of −200 mV to test the reversibility of the catalytic cycle and they were labeled as “Final”.

Infrared studies revealed an additional stretch corresponding to Fe^{II}-CN-Co^{III} at 2116 cm^{-1} with the presence of the intense asymmetric band at 2057 cm^{-1} suggesting the partial oxidation of Co sites in post-catalytic sample [63] (Figure 3.22). After

derivatization of post-catalysis sample with reduction potential, the color turned back to green, which is the color of the pristine sample.

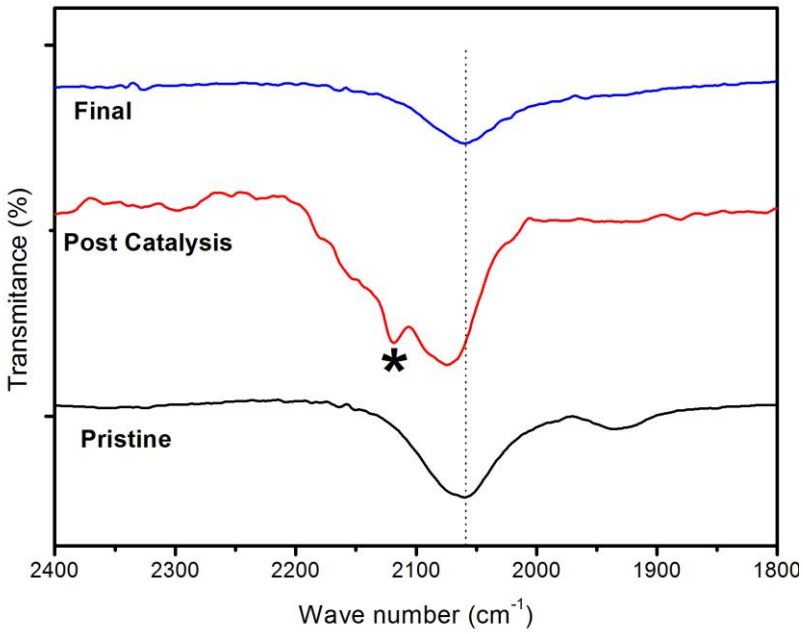

Figure 3.22. IR spectra of $CoFe(CN)_5$-P4VP@FTO electrode before (pristine), after 3 hours bulk electrolysis (post-catalytic), and after a reduction potential of -200 mV is applied for 30 min to the post-catalytic electrode (final) in KPi buffer solution at pH = 7. The peak represented with * is attributed to oxidized Fe^{II}-CN-Co^{III} binding mode.

The XPS studies (Figure 3.23, 3.24), which are carried out to support the IR data suggesting the partial oxidation of Cobalt sites, were also indicated for the pristine, post-catalytic and final samples. XPS of $Co_3(II/III)O_4$ and $Co(NO_3)_2.6H_2O$ were also displayed as reference compounds.

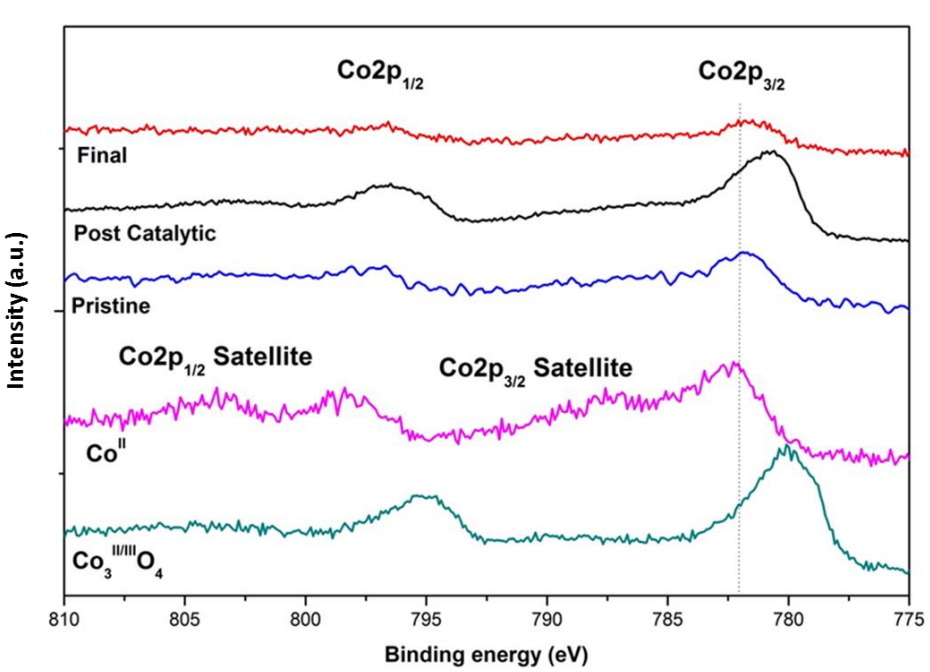

Figure 3.23. XPS of Co2p region for pristine, post-catalytic, and final $CoFe(CN)_5$-P4VP on FTO electrodes.

In the post-catalytic sample, very weak, nearly negligible satellite bands were observed. It indicates that post-catalytic sample is most likely low spin Co(III). So, it can be concluded that the top layer of the electrode exhibits some degree of oxidation in the post catalytic sample, which corresponds well with $Co_3(II/III)O_4$ reference with similar mixed oxidation states. After treatment with reduction potential, the satellite peaks corresponding to Co(II) ion are again observed indicating that the partial oxidation of the surface Co sites is reversible and not permanent [66, 67].

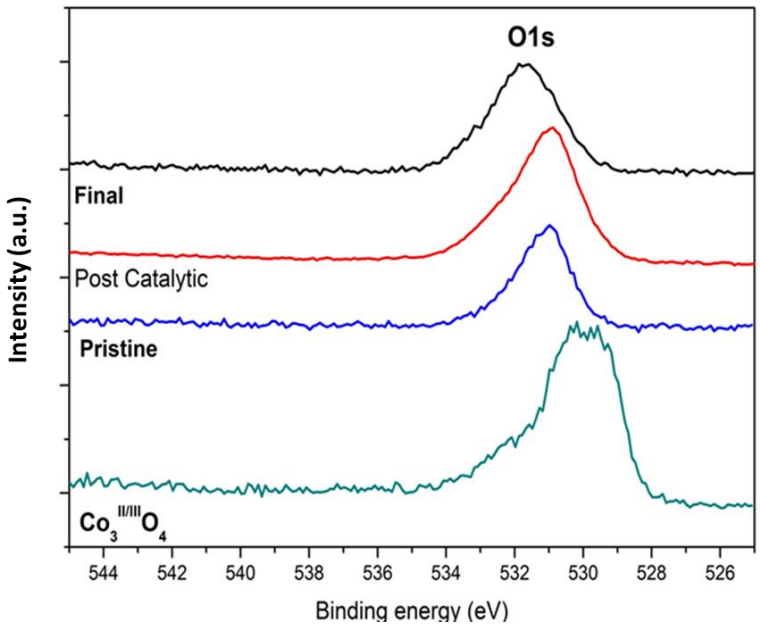

Figure 3.24. XPS of O1s region for pristine, post-catalytic, and final $CoFe(CN)_5$-P4VP on FTO electrodes.

The XPS of the oxygen O1s line was also observed to investigate the stability of electrodes. Spectra of both the original and post-catalytic sample exhibit peaks that are attributed to the surface adsorbed oxygen species. No persistent O1s bands are found at binding energies lower than 530 eV that correspond to lattice oxygen species in either of the samples confirming the absence of any oxide based species before and after catalysis. The decomposition of cyanide based clusters to form any cobalt based oxides was, thus, ruled out based on comparative XPS studies performed on electrodes and reference Co_3O_4 compound [68, 69].

The same trend for IR and XPS studies of $CoFe(CN)_6$@FTO was also observed (Figure 3.25,3.26.3.27). Both infrared and XPS spectra support that the catalyst retains its structure during catalytic process and that oxidation of cobalt sites is a reversible process.

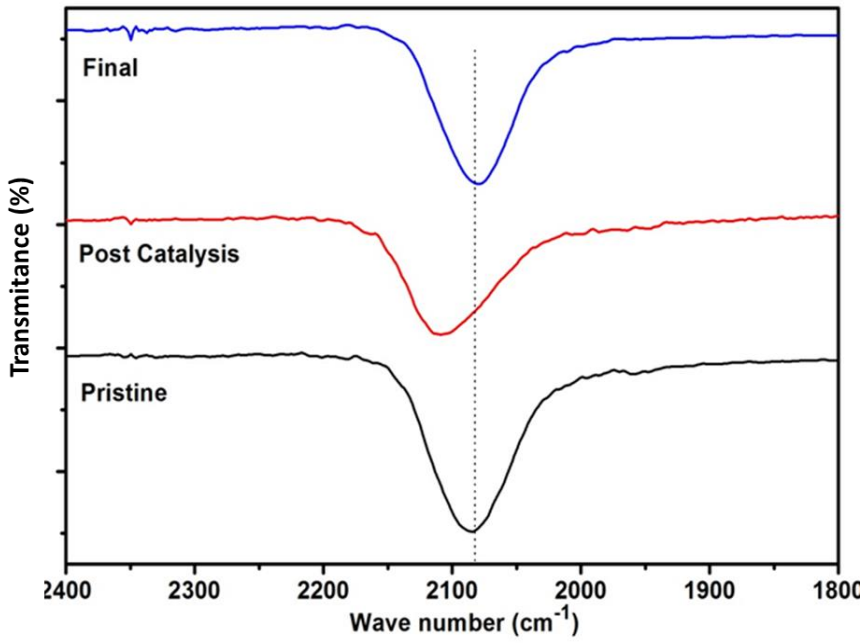

Figure 3.25. IR spectra of $CoFe(CN)_6$@FTO electrode before (pristine), after 3 hours bulk electrolysis (post-catalytic) and final.

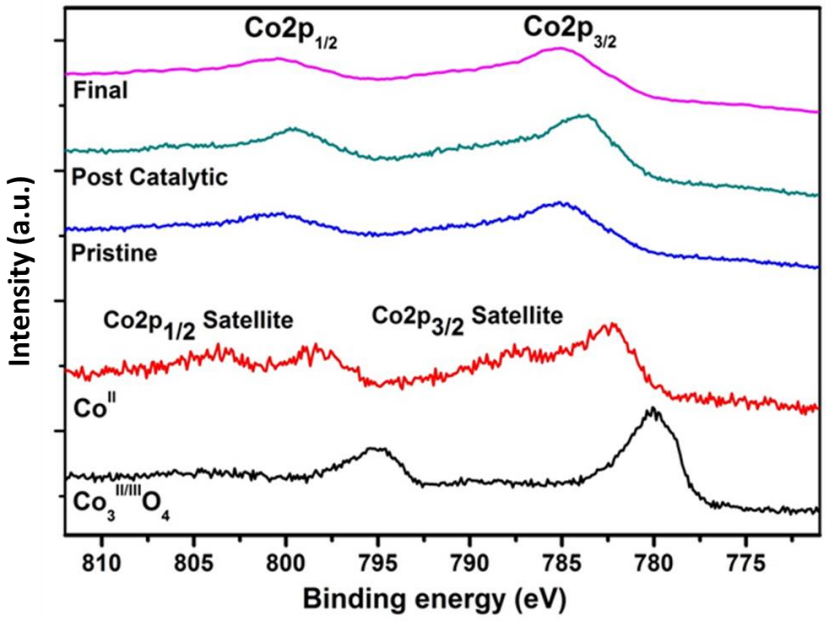

Figure 3.26. XPS of Co2p region for pristine, post-catalytic, and final $CoFe(CN)_6$ on FTO electrodes.

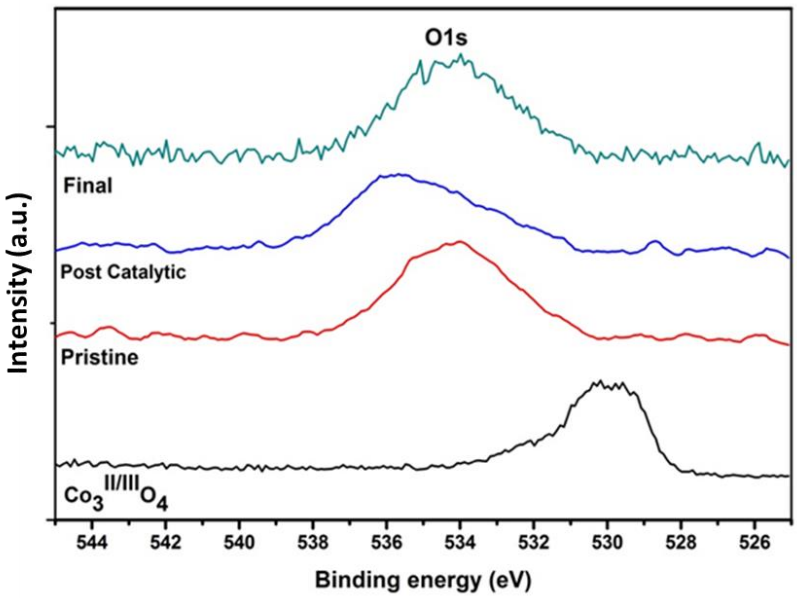

Figure 3.27. XPS of O1s region for pristine, post-catalytic, and final $CoFe(CN)_6$ on FTO electrodes.

Chapter 4

CONCLUSION

Herein, a methodology involving the use of metallopolymers incorporating pentacyanoferrate groups to prepare cobalt cyanide based systems with amorphous nature was employed successfully. Approximately seven fold increase in the number of active cobalt sites with respect to cobalt hexacyanoferrate system could be attributed to the increase in the number defects, thus, the number of active cobalt sites due to amorphous nature of $CoFe(CN)_5$-P4VP. Although $CoFe(CN)_5$-P4VP exhibits a higher Tafel slope than $CoFe(CN)_6$, which could be attributed to the polymeric component of the electrode with insulating behavior, a significant improvement in current densities was observed. A current density of 1 $mA.cm^{-2}$ was obtained at much lower overpotentials (η = 510 mV) with $CoFe(CN)_5$-P4VP modified FTO electrode ,while the same current density needed above η > 600 mV for $CoFe(CN)_6$ electrode. Furthermore, a catalytic onset potential of 360 mV is required to obtain a current density of 55 $\mu A/cm^{-2}$, which is in good agreement with previously studied cobalt based catalysts [14, 70-72]. Comparable turnover frequencies of $CoFe(CN)_6$ and $CoFe(CN)_5$-P4VP electrodes (A TOF value of 2.6×10^{-3} could be achieved at overpotentials of 262 mV and 284 mV, respectively, for $CoFe(CN)_6$@FTO and $CoFe(CN)_5$-P4VP@FTO are mainly as a result of same type of network structural motive including Fe-CN-Co type of binding groups.

Two disciplines of chemistry, pentacyanometal complexes and water oxidation, has been engaged for the first time. The pentacyanometal complexes have well-established chemistry, straightforward synthetic procedures, and rich chemistry due to the diversity of N-donor ligands. The strategy outlined in this project could be used to

introduce many other robust and efficient catalysts to the field of water oxidation. A systematic investigation will be performed in future studies to establish a correlation between structure and catalytic activity of metal pentacyanometalates.

Bibliography

1. Hoffert, M.I., et al., *Energy implications of future stabilization of atmospheric CO2 content.* Nature, 1998. **395**(6705): p. 881-884.

2. *Fundamentals of Materials for Energy and Environmental Sustainability*. 2012, Cambridge University Press.

3. Lewis, N.S. and D.G. Nocera, *Powering the planet: Chemical challenges in solar energy utilization.* Proceedings of the National Academy of Sciences, 2006. **103**(43): p. 15729-15735.

4. Durbin, D.J. and C. Malardier-Jugroot, *Review of hydrogen storage techniques for on board vehicle applications.* International Journal of Hydrogen Energy, 2013. **38**(34): p. 14595-14617.

5. Bockris, J.O.M., *Energy-the Solar Hydrogen Alternative*. 1977: Wiley & Sons.

6. Barber, J., *Photosynthetic energy conversion: natural and artificial.* Chemical Society Reviews, 2009. **38**(1): p. 185-196.

7. Galán-Mascarós, J.R., *Water Oxidation at Electrodes Modified with Earth-Abundant Transition-Metal Catalysts.* ChemElectroChem, 2015. **2**(1): p. 37-50.

8. Dau, H., et al., *The Mechanism of Water Oxidation: From Electrolysis via Homogeneous to Biological Catalysis.* ChemCatChem, 2010. **2**(7): p. 724-761.

9. Blakemore, J.D., R.H. Crabtree, and G.W. Brudvig, *Molecular Catalysts for Water Oxidation.* Chemical Reviews, 2015. **115**(23): p. 12974-13005.

10. Kärkäs, M.D., et al., *Artificial Photosynthesis: Molecular Systems for Catalytic Water Oxidation.* Chemical Reviews, 2014. **114**(24): p. 11863-12001.

11. Sartorel, A., et al., *Shaping the beating heart of artificial photosynthesis: oxygenic metal oxide nano-clusters.* Energy & Environmental Science, 2012. **5**(2): p. 5592-5603.

12. Gerken, J.B., et al., *Electrochemical Water Oxidation with Cobalt-Based Electrocatalysts from pH 0–14: The Thermodynamic Basis for Catalyst Structure, Stability, and Activity.* Journal of the American Chemical Society, 2011. **133**(36): p. 14431-14442.

13. Huang, Z., et al., *Efficient Light-Driven Carbon-Free Cobalt-Based Molecular Catalyst for Water Oxidation.* Journal of the American Chemical Society, 2011. **133**(7): p. 2068-2071.

14. Kanan, M.W. and D.G. Nocera, *In Situ Formation of an Oxygen-Evolving Catalyst in Neutral Water Containing Phosphate and* Co^{2+}. Science, 2008. **321**(5892): p. 1072-1075.

15. Kanan, M.W., Y. Surendranath, and D.G. Nocera, *Cobalt-phosphate oxygen-evolving compound.* Chemical Society Reviews, 2009. **38**(1): p. 109-114.

16. Lutterman, D.A., Y. Surendranath, and D.G. Nocera, *A Self-Healing Oxygen-Evolving Catalyst.* Journal of the American Chemical Society, 2009. **131**(11): p. 3838-3839.

17. Pijpers, J.J.H., et al., *Light-induced water oxidation at silicon electrodes functionalized with a cobalt oxygen-evolving catalyst.* Proceedings of the National Academy of Sciences of the United States of America, 2011. **108**(25): p. 10056-10061.

18. Reece, S.Y., et al., *Wireless Solar Water Splitting Using Silicon-Based Semiconductors and Earth-Abundant Catalysts.* Science, 2011. **334**(6056): p. 645-648.

19. Nocera, D.G., *The Artificial Leaf.* Accounts of Chemical Research, 2012. **45**(5): p. 767-776.

20. Surendranath, Y., M.W. Kanan, and D.G. Nocera, *Mechanistic Studies of the Oxygen Evolution Reaction by a Cobalt-Phosphate Catalyst at Neutral pH.* Journal of the American Chemical Society, 2010. **132**(46): p. 16501-16509.

21. Wasylenko, D.J., et al., *Interrogation of electrocatalytic water oxidation mediated by a cobalt complex.* Chemical Communications, 2012. **48**(15): p. 2107-2109.

22. Wasylenko, D.J., et al., *Electrochemical evidence for catalyticwater oxidation mediated by a high-valent cobalt complex.* Chemical Communications, 2011. **47**(14): p. 4249-4251.

23. Ressnig, D., et al., *Photochemical and electrocatalytic water oxidation activity of cobalt carbodiimide.* Journal of Materials Chemistry A, 2015. **3**(9): p. 5072-5082.

24. Kraft, A. and B. Gesimat GmbH, *On The Discovery and History of Prussian Blue.* Bull. Hist. Chem., 2008. **33**(2): p. 61-67.

25. Herrera, J.M., et al., *Mixed valency and magnetism in cyanometallates and Prussian blue analogues.* Philosophical Transactions of the Royal Society of London A: Mathematical, Physical and Engineering Sciences, 2008. **366**(1862): p. 127-138.

26. Sato, O., et al., *Electric-Field-Induced Conductance Switching in FeCo Prussian Blue Analogues.* Journal of the American Chemical Society, 2004. **126**(41): p. 13176-13177.

27. Kaye, S.S. and J.R. Long, *Hydrogen Storage in the Dehydrated Prussian Blue Analogues $M_3[Co(CN)_6]_2$ (M = Mn, Fe, Co, Ni, Cu, Zn).* Journal of the American Chemical Society, 2005. **127**(18): p. 6506-6507.

28. *Museum of Modern Art (New York City), online database: entry 79802.*

29. Buser, H.J., et al., *The crystal structure of Prussian Blue: $Fe_4[Fe(CN)_6]_3.xH_2O$.* Inorganic Chemistry, 1977. **16**(11): p. 2704-2710.

30. Karyakin, A.A., *Prussian Blue and Its Analogues: Electrochemistry and Analytical Applications.* Electroanalysis, 2001. **13**(10): p. 813-819.

31. Nie, P., et al., *Prussian blue analogues: a new class of anode materials for lithium ion batteries.* Journal of Materials Chemistry A, 2014. **2**(16): p. 5852-5857.

32. Matsumoto, M. and H. Kobayashi, *Hexacyanoferrate-catalyzed oxidation of trimethoxybenzenes to dimethoxy-p-benzoquinones with hydrogen peroxide.* The Journal of Organic Chemistry, 1985. **50**(10): p. 1766-1768.

33. Leal, J.M., B. Garcia, and P.L. Domingo, *Outer-sphere hexacyanoferrate(III) oxidation of organic substrates.* Coordination Chemistry Reviews, 1998. **173**(1): p. 79-131.

34. Pintado, S., et al., *Fast and Persistent Electrocatalytic Water Oxidation by Co–Fe Prussian Blue Coordination Polymers.* Journal of the American Chemical Society, 2013. **135**(36): p. 13270-13273.

35. Goberna-Ferrón, S., et al., *Light-Driven Water Oxidation with Metal Hexacyanometallate Heterogeneous Catalysts.* ACS Catalysis, 2014. **4**(6): p. 1637-1641.

36. Yamada, Y., et al., *High Catalytic Activity of Heteropolynuclear Cyanide Complexes Containing Cobalt and Platinum Ions: Visible-Light Driven Water Oxidation.* Angewandte Chemie International Edition, 2015. **54**(19): p. 5613-5617.

37. Yamada, Y., M. Yoneda, and S. Fukuzumi, *A Robust One-Compartment Fuel Cell with a Polynuclear Cyanide Complex as a Cathode for Utilizing H2O2 as a Sustainable Fuel at Ambient Conditions.* Chemistry-A European Journal, 2013. **19**(35): p. 11733-11741.

38. Brauer, G., *Handbook of Preparative Inorganic Chemistry*. 2 ed. Vol. 1. New York: Academic Press.

39. Macartney, D.H., Rev. Inorg. Chem., 1988. **9**: p. 101-151.

40. Toma, H.E. and J.M. Malin, *Properties and reactivity of some pentacyanoferrate(II) complexes of aromatic nitrogen heterocycles.* Inorganic Chemistry, 1973. **12**(5): p. 1039-1045.

41. Felix, F. and A. Ludi, *Mixed-valence properties of ligand-bridged iron-cyano complexes.* Inorganic Chemistry, 1978. **17**(7): p. 1782-1784.

42. Kamaluddin, M. Nath, and S.W. Deopujari, *Chemical evolution of dehydrogenases: Amino acid pentacyanoferrate (II) as possible intermediates.* Origins of life and evolution of the biosphere. **19**(2): p. 119-132.

43. Jannuzzi, S.A.V., et al., *Supramolecular Interactions between Inorganic and Organic Blocks of Pentacyanoferrate/Poly(4-vinylpyridine) Hybrid Metallopolymer.* The Journal of Physical Chemistry B, 2012. **116**(51): p. 14933-14942.

44. McHale, R., et al., *Dual lanthanide role in the designed synthesis of hollow metal coordination (Prussian Blue analogue) nanocages with large internal cavity and mesoporous cage.* Nanoscale, 2011. **3**(9): p. 3685-3694.

45. Ghasdian, N., et al., *Synthesis of Prussian Blue Metal Coordination Polymer Nanocubes via Cyanoferrate Monomer Design.* Journal of Inorganic and Organometallic Polymers and Materials, 2012. **23**(1): p. 111-118.

46. Uemura, T. and S. Kitagawa, *Prussian Blue Nanoparticles Protected by Poly(vinylpyrrolidone).* Journal of the American Chemical Society, 2003. **125**(26): p. 7814-7815.

47. Shigehara, K., N. Oyama, and F.C. Anson, *Electrochemical responses of electrodes coated with redox polymers. Evidence for control of charge-transfer rates across polymeric layers by electron exchange between incorporated redox sites.* Journal of the American Chemical Society, 1981. **103**(10): p. 2552-2558.

48. Larsson, H., B. Lindholm, and M. Sharp, *Electron transport in quaternized poly(4-vinylpyridine) films containing pentacyanoferrate(II/III) on electrodes. The influence of the binding type of the electroactive complex.* Journal of Electroanalytical Chemistry, 1992. **336**(1–2): p. 263-279.

49. Sharp, M. and H. Larsson, *Studies of the temperature dependence of charge propagation rates in quaternized poly(4-vinylpyridine) polymers containing electrostatically bound and coordinated redox sites.* Journal of Electroanalytical Chemistry, 1995. **386**(1–2): p. 189-195.

50. Roy, X., et al., *Prussian Blue Nanocontainers: Selectively Permeable Hollow Metal–Organic Capsules from Block Ionomer Emulsion-Induced Assembly.* Journal of the American Chemical Society, 2011. **133**(22): p. 8420-8423.

51. Liu, Y. and X. Wang, *Synthesis, characterization, micellization and metal coordination polymerization of pentacyanoferrate-coordinated block copolymers for monodispersed soluble Prussian blue nanospheres.* Polymer Chemistry, 2012. **3**(9): p. 2632-2639.

52. Berrettoni, M., et al., *Synthesis and Characterization of Nanostructured Cobalt Hexacyanoferrate.* The Journal of Physical Chemistry C, 2010. **114**(14): p. 6401-6407.

53. Dehnicke, K., *The Chemistry of Cyano Complexes of the Transition Metals. Organometallic Chemistry - A Series of Monographs. Von A. G. Sharpe. Academic Press, London-New York-San Francisco 1976. 1. Aufl., XI, 302 S., geb. £ 10.40.* Angewandte Chemie, 1976. **88**(22): p. 774-774.

54. Gliemann, G., *K. Nakamoto: Infrared and Raman Spectra of Inorganic and Coordination Compounds. John Wiley and Sons, New York, Chichester, Brisbane, Toronto 1978. 3. Aufl., XV, 448 Seiten mit 109 Abbildungen und 95 Tabellen. Preis:*

$31, 15. Berichte der Bunsengesellschaft für physikalische Chemie, 1978. **82**(11): p. 1263-1263.

55. Zhou, X., et al., *Interpolymer complexation between poly(vinylphosphonic acid) and poly(vinylpyridine)s.* Polymer, 1997. **38**(21): p. 5333-5338.

56. Ruokolainenl, J., et al. *Self-organized nanostructures of poly (4-vinylpyridine), polyaniline and polyamides due to metal complexation*. in *Macromol. Symp*. 2002.

57. Kettle, S.F.A., et al., *The Vibrational Spectra of the Cyanide Ligand Revisited. Bridging Cyanides.* Inorganic Chemistry, 2007. **46**(7): p. 2409-2416.

58. Hrepic, N.V. and J.M. Malin, *Electron transfer and ligand substitution reactions of the ion pentacyano(4-aminopyridine)ferrate(II).* Inorganic Chemistry, 1979. **18**(2): p. 409-413.

59. Bleuzen, A., et al., *Photoinduced Ferrimagnetic Systems in Prussian Blue Analogues $CI_xCo_4[Fe(CN)_6]_y$ (CI = Alkali Cation). 1. Conditions to Observe the Phenomenon.* Journal of the American Chemical Society, 2000. **122**(28): p. 6648-6652.

60. Biesinger, M.C., et al., *Resolving surface chemical states in XPS analysis of first row transition metals, oxides and hydroxides: Cr, Mn, Fe, Co and Ni.* Applied Surface Science, 2011. **257**(7): p. 2717-2730.

61. Del Pilar-Albaladejo, J. and P.K. Dutta, *Topotactic Transformation of Zeolite Supported Cobalt(II) Hydroxide to Oxide and Comparison of Photocatalytic Oxygen Evolution.* ACS Catalysis, 2014. **4**(1): p. 9-15.

62. Burke, M.S., et al., *Cobalt–Iron (Oxy)hydroxide Oxygen Evolution Electrocatalysts: The Role of Structure and Composition on Activity, Stability, and Mechanism.* Journal of the American Chemical Society, 2015. **137**(10): p. 3638-3648.

63. Lezna, R.O., et al., *Cobalt Hexacyanoferrate: Compound Stoichiometry, Infrared Spectroelectrochemistry, and Photoinduced Electron Transfer.* The Journal of Physical Chemistry B, 2002. **106**(14): p. 3612-3621.

64. Zanello, P., *Inorganic Electrochemistry: Theory, Practise and Applications*. 2003, Cambridge, UK: The Royal Society of Chemistry.

65. Bard, A.J.F., L. R. , *Electrochemical Methods: Fundamentals and Applications*. 2001: John Wiley & Sons, Inc.

66. Chen, H., et al., *Cobalt–Salen Complexes as Catalyst Precursors for Electrocatalytic Water Oxidation at Low Overpotential.* The Journal of Physical Chemistry C, 2015. **119**(17): p. 8998-9004.

67. McIntyre, N.S. and M.G. Cook, *X-ray photoelectron studies on some oxides and hydroxides of cobalt, nickel, and copper.* Analytical Chemistry, 1975. **47**(13): p. 2208-2213.

68. Petitto, S.C., et al., *Cobalt oxide surface chemistry: The interaction of CoO(1 0 0), Co3O4(1 1 0) and Co3O4(1 1 1) with oxygen and water.* Journal of Molecular Catalysis A: Chemical, 2008. **281**(1–2): p. 49-58.

69. Biesinger, M.C., et al., *X-ray photoelectron spectroscopic chemical state quantification of mixed nickel metal, oxide and hydroxide systems.* Surface and Interface Analysis, 2009. **41**(4): p. 324-332.

70. Ahn, H.S. and T.D. Tilley, *Electrocatalytic Water Oxidation at Neutral pH by a Nanostructured Co(PO3)2 Anode.* Advanced Functional Materials, 2013. **23**(2): p. 227-233.

71. Kim, H., et al., *Coordination tuning of cobalt phosphates towards efficient water oxidation catalyst.* Nat Commun, 2015. **6**: p. 1-11.

72. Smith, R.D.L., et al., *Photochemical Route for Accessing Amorphous Metal Oxide Materials for Water Oxidation Catalyst,* 2013. **340**: p. 60-63.